### RESEARCH ARTICLE



# Multifaceted approach toward mapping out the anticancer properties of small molecules via in vitro evaluation on melanoma and nonmelanoma skin cancer cells, and in silico target fishing

Samuel T. Boateng<sup>1</sup> | Tithi Roy<sup>1</sup> | Mercy E. Agbo<sup>2</sup> | Md Ashiq Mahmud<sup>1</sup> | Sergette Banang-Mbeumi<sup>1</sup> | Roxane-Cherille N. Chamcheu<sup>1</sup> | Rajesh K. Yadav<sup>1</sup> | Marion Bramwell<sup>1</sup> | Long K. Pham<sup>1</sup> | Danny D. Dang<sup>1</sup> | Keith E. Jackson<sup>1</sup> | Bolni Marius Nagalo<sup>3,4</sup> | Ronald A. Hill<sup>1</sup> | Tatiana Efimova<sup>5</sup> | Jean Fotie<sup>2</sup> | Jean Christopher Chamcheu<sup>1,6</sup> |

# Correspondence

Jean Christopher Chamcheu, School of Basic Pharmaceutical and Toxicological Sciences, College of Pharmacy, University of Louisiana – Monroe, Monroe, LA 71209-0497, USA. Email: chamcheu@ulm.edu

Jean Fotie, Department of Chemistry and Physics, Southeastern Louisiana University, Hammond, LA 70402-0878, USA.

Email: jean.fotie@southeastern.edu

### **Funding information**

Edward G. Schlieder Educational Foundation; Louisiana Biomedical Research Network, Grant/Award Number: 3P20GM103424-18S1; Louisiana Board of Regents, Grant/ Award Number: (2021-24)-RD-A-22; National Institute of General Medical Sciences of the National Institutes of Health, Grant/Award Number: P2O GM103424-18; US National Science Foundation; University of Louisiana Monroe; University of Louisiana at Monroe (ULM) College of Pharmacy

### **Abstract**

Melanoma and nonmelanoma skin cancers are among the most prevalent and most lethal forms of skin cancers. To identify new lead compounds with potential anticancer properties for further optimization, in vitro assays combined with insilico target fishing and docking have been used to identify and further map out the antiproliferative and potential mode of action of molecules from a small library of compounds previously prepared in our laboratory. From screening these compounds in vitro against A375, SK-MEL-28, A431, and SCC-12 skin cancer cell lines, 35 displayed antiproliferative activities at the micromolar level, with the majority being primarily potent against the A431 and SCC-12 squamous carcinoma cell lines. The most active compounds 11 (A431:  $IC_{50} = 5.0 \,\mu\text{M}$ , SCC-12:  $IC_{50} = 2.9 \,\mu\text{M}$ , SKMEL-28:  $IC_{50} = 4.9 \,\mu\text{M}$ , A375:  $IC_{50} = 6.7 \,\mu\text{M}$ ) and **13** (A431:  $IC_{50} = 5.0 \,\mu\text{M}$ , SCC-12:  $IC_{50} = 3.3 \,\mu\text{M}$ , SKMEL-28:  $IC_{50} = 13.8 \,\mu\text{M}$ , A375:  $IC_{50} = 17.1 \,\mu\text{M}$ ), significantly and dose-dependently induced apoptosis of SCC-12 and SK-MEL-28 cells, as evidenced by the suppression of Bcl-2 and upregulation of Bax, cleaved caspase-3, caspase-9, and PARP protein expression levels. Both agents significantly reduced scratch wound healing, colony formation, and expression levels of deregulated cancer molecular targets including RSK/Akt/ERK1/2 and S6K1. In silico target prediction and docking studies using the SwissTargetPrediction web-based tool suggested that CDK8, CLK4, nuclear receptor ROR, tyrosine protein-kinase Fyn/

<sup>&</sup>lt;sup>1</sup>School of Basic Pharmaceutical and Toxicological Sciences, College of Pharmacy, University of Louisiana – Monroe, Monroe, Louisiana, USA

<sup>&</sup>lt;sup>2</sup>Department of Chemistry and Physics, Southeastern Louisiana University, Hammond, Louisiana, USA

<sup>&</sup>lt;sup>3</sup>Department of Pathology, University of Arkansas for Medical Sciences (UAMS), Little Rock, Arkansas, USA

<sup>&</sup>lt;sup>4</sup>The Winthrop P. Rockefeller Cancer Institute, University of Arkansas for Medical Science (UAMS), Little Rock, Arkansas, USA

 $<sup>^5</sup>$ Department of Biomedical Engineering, Northwestern University, Chicago, Illinois, USA

<sup>&</sup>lt;sup>6</sup>Department of Pathology and Translational Pathobiology, Louisiana State University Health Sciences Center, Shreveport, Louisiana, USA

(COP), Grant/Award Number: 5CALHN-260615

LCK, ROCK1/2, and PARP, all of which are dysregulated in skin cancers, might be prospective targets for the two most active compounds. Further validation of these targets by western blot analyses, revealed that ROCK/Fyn and its associated Hedgehog (Hh) pathways were downregulated or modulated by the two lead compounds. In aggregate, these results provide a strong framework for further validation of the observed activities and the development of a more comprehensive structure–activity relationship through the preparation and biological evaluation of analogs.

#### **KEYWORDS**

anticancer activity, apoptosis, in silico target(s) prediction, melanoma and nonmelanoma skin cancer cells, ROCK/Fyn and Hedgehog (Hh) pathway as potential targets

## 1 | INTRODUCTION

Skin cancer is among the most prevalent types of cancer in the United States (Guy, Machlin, et al., 2015; Guy, Thomas, et al., 2015), and it is estimated that one in five Americans will develop skin cancer in their lifetime (Miller et al., 2022; Siegel et al., 2022), with approximately 9500 people diagnosed every day (Miller et al., 2022; Paulson et al., 2020; Siegel et al., 2022). While nonmelanoma skin cancer (NMSC), including basal cell carcinoma (BCC) and squamous cell carcinoma (SCC), is the most common type of skin cancer (Miller et al., 2022; Siegel et al., 2022), the rate of melanoma has been rising rapidly in the United States over the past decades, with the vast majority of skin cancer deaths arising from melanoma (Beroukhim et al., 2020; Miller et al., 2022; Siegel et al., 2022). It is well accepted that most melanoma cases are attributable to UV exposure (Agbai et al., 2014; Arnold et al., 2018; Islami et al., 2020), including sunburns and prolonged use of tanning beds (An et al., 2021; Colantonio et al., 2014; Dennis et al., 2008; Lee, 2019).

While surgical tumor excision is one of the most effective therapeutic approaches for the early stages of skin cancers, it can result in disfigurement, requiring further skin grafts to cover the defects, not to mention the possibility of metastasis and tumor recurrence in many cases (Mulvaney & Schmults, 2020; Pavel et al., 2020; Robertson et al., 2018). Significant advances have been made toward a better understanding of mechanisms through which melanoma and nonmelanoma skin cancers are triggered and sustained. As a result, arresting proliferation or inducing programmed cell death in tumors has become an alternative and an effective cancer therapy option (Ascierto & Garbe, 2020; Hwang et al., 2020). Several kinases, including RAF1 (Donati et al., 2020; Jeric et al., 2016), ROCK1 and 2 (Chang et al., 2018; Kaczorowski et al., 2020), serine-threonine protein

kinase (CHK1) (Tho et al., 2012; Wang et al., 2018), tyrosine-protein kinase (FYN) (Martens et al., 2018), tyrosine protein kinase (LCK) (Fathi et al., 2013), and dual specificity protein kinase (CLK4) are well known to play critical roles in skin tumorigenesis. SK-MEL-28 (one of a series of melanoma cell lines established from patient-derived tumor samples) and A375, both used in this study, are well known to harbor BRAF V600E driver mutation and wild-type N-RAS (Brummer et al., 2006). On the other hand, nicotinamide adenine dinucleotide (NAD)-biosynthetic enzyme (nicotinamide phosphoribosyltransferase, also known as NAMPT) was shown to be a driving factor in a resistance associated with serine-threonine protein kinase B-RAF (BRAF)-mutated metastatic melanoma, one of the highly aggressive types of skin cancer (i.e., BRAF inhibitor resistance) (Audrito et al., 2020; Brandl et al., 2019). Further studies revealed that NAMPT over-expression is necessary and sufficient to recapitulate the BRAFi-resistant phenotype plasticity (Audrito et al., 2020). PI3K/RAC alpha serine/threonine protein kinase (AKT)/mTOR signaling pathway has also been shown to be over-activated in some types of skin cancers (Tu et al., 2019), with the antiproliferative activity of some phenolic compounds against SK-MEL-28 cancer cells attributed to the downregulation of the PI3K/AKT/mTOR signaling pathway, which induces a mitochondrial-dependent apoptosis (Won et al., 2020). Moreover, the poly(ADP-ribose) polymerase (PARP) (Murahari & Yergeri, 2014; Pisano et al., 2021), phosphodiesterase type 5 (Han et al., 2018; Tang et al., 2017), orphan nuclear receptor LRH-1 (Chen et al., 2020; Vogeley et al., 2019), nuclear receptor RORgamma (Brozyna et al., 2016, 2019), matrix metallopeptidase 9 (MMP9) (Aranha et al., 2021), NAD-dependent deacetylase Sirtuin 2 (Wang et al., 2014), and cholesterol ester transfer protein (Nair et al., 2015) are all believed to play important roles in skin carcinogenesis. All these

proteins, enzymes, kinases, proteases, oxidoreductases, phosphodiesterases, and erasers are among the 2600 protein targets (2100 of which are human), and the reported activities for more than 376,000 compounds involving an excess of 580,000 reported interactions, comprised in the SwissTargetPrediction tool (Daina et al., 2017, 2019; Gfeller et al., 2014).

As part of a continuing effort to introduce new molecular scaffolds and entities into the cutaneous cancer treatment pipeline, our research group recently showed that fisetin and its analogs inhibit the PI3K/Akt/mTOR and MAPK, and effected key pathways in organotypic human inflammatory skin and melanoma models (Chamcheu, et al., 2019; Roy et al., 2021a, 2021b) as well as c-Kit, CDK2, and mTOR kinases in melanoma and nonmelanoma skin cancers (Roy et al., 2021a, 2021b). Herein, we used a combination of in vitro assays, in silico target fishing and docking studies to identify and outline the antiproliferative activity of molecules from a small library of compounds previously prepared in our laboratory as part of the investigation of the malaria parasite biochemistry relevant to the mechanism of quinoline-derived antimalarial drugs. Among them, 35 compounds were identified to possess an optimizable antiproliferative activity when evaluated in vitro against melanoma (A375 and SK-MEL-28) and nonmelanoma (A431 and SCC-12) skin cancer cell lines. In silico studies using the SwissTargetPrediction tool indicated that many of these compounds have favorable physicochemical properties and in combination with docking predictions, suggested that CDK8, CLK4, nuclear receptor ROR, tyrosine protein-kinase Fyn/LCK, ROCK1/2, and PARP might be prospective molecular targets for the two most active compounds (11 and 13). Scratch woundhealing and colony formation functional/phenotypic assays indicated that compounds 11 and 13 exert their activity by interfering with the apoptotic pathways. At the same time, western blot analyses suggested that ROCK/Fyn and the Hedgehog (Hh) pathway might be involved in the mechanisms of the action of the two lead compounds.

# 2 MATERIALS AND METHODS

# 2.1 | Chemistry

The compounds screened in this manuscript were all previously prepared in our lab, and the procedures used for their synthesis are fully described in the Appendix S1, together with all the characterization data. NMR data were collected on a Bruker AscendTM® 400 spectrometer operating at 400 MHz for <sup>1</sup>H and 100 MHz for <sup>13</sup>C.

The concentration of all samples was about 20 to 50 mg in 0.5 mL of CDCl<sub>3</sub>. The NMR data were recorded at 400 K, with chemical shifts ( $\delta$ ) reported in parts per million (ppm) relative to TMS ( $\delta_{\rm H}$  0.00 and  $\delta_{\rm C}$  0.0) used as the internal standard, or residual chloroform (δH 7.28 and δC 77.2), and coupling constants (J) in hertz. The multiplicity is as follows: s = singlet, d = doublet, t = triplet, q = quartet,  $q^* = quintet$ , m = multiplet. Reaction mixtures were monitored by TLC using silica gel 60 F254 plates or by a 200-MS Varian GC/MS ion trap mass spectrometer on which all the GC-MS spectra were recorded. The product(s) from each reaction was purified on a Teledyne ISCO RF200 CombiFlash, using a 40 g RediSepRF silica column, or by gravity and flash column chromatography using type 60A silica gel (60–230 mesh). Single crystals of various samples suitable for x-ray structure determination were mounted on the tip of a glass fiber using silicon grease, and the intensity data were recorded at 90 K on an STOE IPDS-2T diffractometer using graphite-monochromated MoKa radiation ( $\lambda = 0.71073 \,\text{Å}$ ). Intensity data for all crystals were readily indexed and the structures were solved by direct method and refined by full-matrix least-squares techniques in the SHELTXL package of programs. The structure solutions reveal the positions of all non-hydrogen atoms within the crystal with some of the hydrogen positions. In subsequent refinement steps, the positions of the remaining hydrogen atoms were deduced from different Fourier syntheses. The Diamond software was utilized to create graphic representations of the crystal structures with ellipsoid representations (50% probability level) for all non-hydrogen atoms.

All chemicals and solvents were purchased from major chemical suppliers and were used without further purification unless stated otherwise.

# 2.2 | In vitro biological evaluation

# 2.2.1 Antibodies, chemicals, and reagents

3-(4,5-Dimethylthiazol-2-yl)-2,5-diphenyltetrazoli um bromide (MTT), dimethyl sulfoxide (DMSO) and 4′,6-diamidino-2-phenylindole (DAPI-#DUO82040), in situ mounting media and bovine serum albumin (BSA) were purchased from Sigma–Aldrich Chemical Company and MP Biomedicals, respectively. Antibodies for immunoblotting and immunocytochemistry, including caspase 3 (9662S), caspases 9 (#9502), Bcl-2 (2876S), Bax (2772S), β-Actin (13E5) Rabbit mAb #4970, GAPDH (D16H11) #5174S, pS6 (Ser235/236) #4858, a pan antibody mix of Phospho-Akt (Ser473) (D9E) XP® Rabbit mAb #4060, Phospho-p90RSK, Phospho-p44/42 MAPK (Erk 1/2) (Thr202/Tyr204), PARP Antibody #9542, Phospho-S6

Ribosomal Protein Detection Cocktail I (5301S), Rock-1 (C8F7) Rabbit mAb #4035I, Rock-2 (D1B1) Rabbit mAb #9029S, Fyn Rabbit mAb #4023S, LCK Rabbit mAb #2752S, GLI-1 (V812) Rabbit mAb #2534S, SHH (C9C5) Rabbit mAb #2207P, and horseradish peroxidase-conjugated (HRP) anti-mouse and anti-rabbit secondary antibodies were all obtained from Cell Signaling Technologies. GLI-2 Specific Polyclonal Rabbit antibody #18989-1-AP was purchased from Protein Technology (Proteintech Group, Inc.). Invitrogen Goat anti-Mouse IgG (H+L) Cross-Adsorbed Secondary Antibody, Texas Red-X and Goat anti-Rabbit IgG (H+L) Highly Cross-Adsorbed Secondary Antibody, Alexa Fluor™ Plus 488, Radioimmunoprecipitation assay (RIPA) buffer, Pierce Bicinchoninic acid (BCATM) protein assay kit, and the SuperSignal™ West Pico PLUS Chemiluminescent substrate detection system were purchased from ThermoFisher Scientific. Mini-protean precast Tris-Glycine Gels (TGX) were from Bio-Rad (Bio-Rad Laboratories Inc.). A 2% (w/v) Aqueous Solution of Gentian Violet and crystal violet were from Ricca Chemical Company. Dulbecco's modified Eagle's medium (DMEM) and Roswell Park Memorial Institute Medium (RPMI 1640) were from Corning. Epi-Life® Growth Medium with 60 µM calcium and Cascade Biologist human keratinocyte growth supplement (HKGS) 100X (S-001-5) were from Life Technologies. The Dulbecco's phosphate-buffered saline (DPBS), phosphate buffer saline (PBS) 1X, defined trypsin inhibitor (DTI) 1X (R007-100), trypsin EDTA 0.25%, 1X (R25200-072), Trypsin neutralizer (TN) 1X (R-002-100), penicillin-streptomycin (Pen Strep, 15140-122) (PEST) 100X were purchased from Gibco, ThermoFisher Scientific, and human keratinocyte growth supplement (HKGS) 100X (S-001-5) from Cascade Biologist were procured from VWR Corporation. USDAapproved Origin Fetal Bovine Serum (FBS) was procured from VWR Seradigm Life Science. The organic solvents including, ethanol (6183-10) and methanol (BDH 1135-4LP), were acquired from Macron Chemicals and VWR, respectively.

# 2.2.2 | Cell lines, cell cultures, cytotoxicity, and viability evaluation assay

Human-derived GFP-expressing melanoma A375, and epidermoid carcinoma A431 cell lines were purchased from Angio-Proteomie. Cells of human melanoma carcinoma SK-MEL-28 lines were acquired from American Type Culture Collection (ATCC). The human immortalized keratinocyte cell line (N/TERT1), (Dickson et al., 2000) was generously gift from Dr. Ellen van den Bogaard (Radboud University Nijmegen, Netherlands) to Dr. Chamcheu. These cells were cultured and maintained in Epi-Life®

Growth Medium supplemented with (low) 60 µM calcium and cascade Biologist human keratinocyte growth supplement (HKGS). Human cutaneous SCC cell line SCC-12 (Rheinwald & Beckett, 1981) was generously provided by Dr. James G. Rheinwald to Dr. Efimova. Except for SK-MEL-28, which was cultured in an RPMI-1640 medium supplemented with 5% FBS, all other human immortalized cell lines were grown and maintained in DMEM containing varying percentages of FBS: 5% FBS for A431 and SCC-12 lines, and 10% FBS for A375. All culture media were routinely supplemented with 1% PEST 100X (100 U/mL penicillin and 100 μg/mL streptomycin), and cells were cultured in incubators maintained at 37°C under an atmosphere of 95% humidity, 20% O2 and 5% CO<sub>2</sub>. The growth media of incubated cells were changed every 2-3 days until they attained 70%-80% confluence, after which they were subcultured for experiments and/ or re-passaging. DMSO was used as a vehicle to prepare a 10 mM stock solution of the test compounds. Control cells were treated with the vehicle (DMSO) at concentrations (0.01%–0.2%), not affecting cell viability. From these 10 mM stock solutions prepared in DMSO, escalating concentrations were prepared using the corresponding cell growth media as a diluent, and the cells (65%-75% confluent) were treated with (0-40 µM) or without the drug in sext-to octuplicate and incubated for 48 h. All treatment protocols and controls were prepared as previously described (Roy et al., 2021a, 2021b).

The MTT assay method was performed to assess the potency and cytotoxic influence of the test compounds against two cutaneous melanoma (A375 and SK-MEL-28) and two nonmelanoma (A431 and SCC-12) skin cancer cell lines in addition to a control immortalized normal human epidermal keratinocytes (NTERT/1) cell line. Briefly, exponentially growing parent passage cells at 70%-85% confluency were harvested, washed, counted using a hemocytometer, and individually seeded at a density of  $2-5\times10^3$  cells/well in a 96-well plate in 200 µL of their respective growth media, incubated and monitored until reaching their logarithmic growth phase at over 70% confluent before treatment. All experimental treatment concentrations were repeated at least in 8-10 wells, and the experiment was repeated six to eight times. Subsequently, the cells were harvested following the MTT protocol as previously described (Chamcheu, et al., 2019), with absorbance measured at 562 nm wavelength using a SynergyLX, multimode microplate reader (BioTek Instruments Inc.). The results from escalating concentration of each test and control (cisplatin) agent were analyzed using the zero drug control groups as the relative comparator and are expressed as a percentage following the equation: [(absorbance in treatment group/absorbance in control) × 100%]. GraphPad Prism software version 9.3 (GraphPad Software,

Inc.) was then used to compute the various  $IC_{50}$  values as earlier described (Roy et al., 2021a, 2021b).

# 2.2.3 | Colony formation assay

This assay was performed to demonstrate the colony formation potential of the active compounds on SCC-12 and SK-MEL-28 cell lines, following a previously described protocol (Roy et al., 2021a, 2021b). Briefly, 3000 viable cells treated with compounds 11 or 13 at varying concentrations (0,  $\frac{1}{2}IC_{50}$ ,  $IC_{50}$ , and  $\frac{1}{2}IC_{50}$ ) for 48 h in a T-25 flask were harvested and seeded into a 10 cm<sup>2</sup> plate in quadruplicates in respective drug-free growth medium. Plates were monitored with routine media change every alternate day for 10-14days until control cells reached about 90% confluency or cell plates formed about 50–150 colonies. The cell plates were then harvested by washing twice in 1×PBS, followed by fixing and staining in a submerged solution containing 0.5% gentian violet staining agent in 64% (v/v) methanol and 4% paraformaldehyde (4% PFA) for 45–60 min at room temperature. Stained cells were gently washed in tap water until the solution became clear and were air-dried and imaged with a Nikon D7500 camera. Colonies were counted and analyzed using the count and Plot Histograms of Colony Size (countPHICS) analysis tool99 and GraphPad Prism software version 9.1 (GraphPad Software, Inc.), respectively. Statistical analyses of the data provided values for the mean  $\pm$  SD of three independent experiments, comparing each treatment group to the DMSO group: p < .05, \*\*p < .01, \*\*\*p < .001.

# 2.2.4 | Immunofluorescence staining and immunocytochemical analysis of cell morphology by (β-actin cytoskeleton reorganization) and apoptosis (caspase-3 activation)

Immunofluorescence analysis was employed to detect morphological and biochemical changes associated with the expression of an apoptosis marker (caspase 3) and the cell actin cytoskeleton reorganization following the treatment of cultured cells. Briefly, cells pre-seeded into an 8-well chamber slide were treated with escalating concentrations (0,  $\frac{1}{2}IC_{50}$ ,  $IC_{50}$  and  $1\frac{1}{2}IC_{50}$ ) of the test compounds 11 or 13 for 48 h. The cells were washed and fixated using 4% PFA in PBS pH 7.4 for 20–30 min at room temperature, followed by permeabilization in 0.1% Triton X-100 stabilization buffer for 5 min and washing three times with cold 1×PBS. Nonspecific binding was reduced using a blocking buffer with 1%BSA for 0.5–1 h. The cells were added to the respective primary antibodies ( $\beta$ -Actin or Caspase-3 at

[1:1000 dilution]) for fluorescence staining, and cell slides were incubated overnight at 4°C. Slides were subsequently washed thrice and incubated with Cross-Adsorbed Texas Red- Goat Anti-mouse IgG (H+L) (dilution 1:600) and Alexa fluor™ Plus 488 Goat Anti-rabbit IgG (H+L) (dilution 1:1000) Secondary Antibodies for 2h at room temperature in the dark. Slides were rewashed and mounted using in situ mounting media containing phalloidin and 4′,6-diamidino-2-phenylindole (DAPI). The mounted slides were visualized and imaged using an inverted fluorescence microscope (Olympus IX71 equipped with a DP71 digital camera) at 10× and 20× magnification. The images captured were processed using the cellSens Imaging Software V3.2, and each experiment was per-

# 2.2.5 | In vitro wound-healing assay

formed three times (Chamcheu, et al., 2019).

The scratch wound-healing assay was performed to evaluate the ability of compound 11 or 13 to limit the migration and wound closure using a previously described protocol (Chamcheu, et al., 2019; Roy et al., 2021a, 2021b). Briefly, a 24-well plate seeded with cells was incubated until a fully confluent monolayer of cells was attained. This layer was disrupted by scratching a straight line across the center using a sterile 200 µL Gilson pipette tip. The plated cells were washed gently to remove debris and detached cells, and then treated with compound 11 or 13 at escalating concentrations (0,  $\frac{1}{2}IC_{50}$ ,  $IC_{50}$ , and  $\frac{1}{2}IC_{50}$ ). At times 0h, 24h, and 48h, the scratch wound and reepithelialization areas were imaged using an inverted phasecontrast microscope (Olympus IX51, Olympus America Inc.) attached to an Infinity 2 digital camera processing with Infinity Analyze software version 6.5.6 (Teledyne Lumenera) and Adobe Photoshop. The ImageJ software package (NIH, Bethesda, MD) was then used to measure the wounded area covered for each treatment group at 24h and 48h versus time 0h (Chamcheu, et al., 2019; Roy et al., 2021a, 2021b).

# 2.2.6 | Preparation of cell lysates, western blot assay, and analysis

Cell lysate preparation and immunoblotting were performed. Briefly, lysates were prepared after subjecting  $3\times10\,\mathrm{cm}^2$  plates seeded with about 3000 cells each and treated with varying concentrations (0, ½IC<sub>50</sub>, IC<sub>50</sub>, and ½IC<sub>50</sub>) of compounds for 48 h, following the reference protocol (Chamcheu, et al., 2019; Roy et al., 2021a, 2021b). After treatment with compound 11 or 13, the cell growth medium was aspirated, and the cells were

harvested after washing in cold 1×PBS (pH 7.4), and whole-cell, cytosolic, and nuclear lysates were prepared as described earlier (Chamcheu, et al., 2019; Roy et al., 2021a, 2021b). Briefly, cells were lysed by incubating in cell lysis RIPA buffer supplemented with protease and phosphatase inhibitors; 1 mM PMSF (phenylmethylsulfonyl fluoride), 10 mM RIPA buffer, 1 mM protease inhibitor cocktail (1 mM EDTA, 20 mM NaF, 0.5% NP-40, 1% Triton X-100) (Roche) and 0.5% Na<sub>3</sub>VO<sub>4</sub> on ice. The homogenate was then centrifuged at 14,000 g for 25 min at 4°C, the supernatant was collected, and the cleared lysate protein concentration was quantified using the BCA protein assay kit (Thermo Scientific) according to the manufacturer's protocol. A readout was obtained using the Eppendorf BioPhotometer D30, and aliquots were also withdrawn either for immediate use or for storage at -80°C for later use for western blot assay as earlier described (Chamcheu, et al., 2019; Roy et al., 2021a, 2021b).

Western blotting was carried out, with analysis aimed at identifying potential mechanisms and targeted pathways accounting for the observed biological responses to treatments with compounds 11 or 13, following previously described protocols. Accordingly, lysates were denatured in 2X Laemmli sample buffer and loaded onto gels (so as to resolve equal amounts of protein, 25g per lane) using a KD 4-12% polyacrylamide ready mini-PROTEAN TGX gels electrophoresis apparatus, which effects separation based on molecular weight and overall molecular charge differentials. The resolved proteins were transferred into a nitrocellulose filter membrane using a Trans-Blot Turbo Transfer Pack. The presence of proteins was indicated by using a ponceau staining before proceeding to washes (2X) under tap water and TBS-T wash buffer. Unspecific epitopes in the membrane were blocked with 5% BSA (for phospho-protein targets) or 5% nonfat dry milk/1% Tween 20; in 20 mM Tris-buffered saline (TBS or wash buffer) at room temperature on a rotating shaker for 45 min. The membranes were incubated overnight at 4°C or for 2h at room temperature, in blocking solutions containing the corresponding monoclonal or polyclonal primary antibodies (1:250 to 1:1000 dilution). Blots were then washed three times (5 min each) with PBST and incubated in anti-mouse or anti-rabbit horseradish-peroxidase (HRP) conjugated secondary antibody (1:2000 dilution). Afterward, blots were rewashed three times (5 min each) with PBST and MilliQ-water, exposed to Enhanced Chemiluminescence Plus West Pico for 5 min, and autoradiographed in a BioRad Gel-Doc System (Bio-Rad Laboratories). The loading consistency was verified by stripping and re-probing blots with primary monoclonal antibody tagging housekeeping proteins (β-actin, GAPDH, and Rab11) following previously described procedures (Chamcheu, et al., 2019; Roy et al., 2021a, 2021b). The bands were then visualized and imaged using the Bio-Rad ChemiDoc<sup>TM</sup> detection system. Densitometry was done using Quantity One, the BioRad digitized scientific imaging analysis software program. The Rab11 and  $\beta$ -actin densitometric readouts were used for normalization, linear ranges of band densities were established through multiple blot exposures, and the analysis and data presented were based on three different experiments. The resulting data were analyzed for statistically significant differences according to one-way ANOVA as computed with the GraphPad Prism software package (version 9.3.1) (Chamcheu, et al., 2019).

# 2.3 | In silico screening assays

# 2.3.1 Target prediction methodology

The SwissTargetPrediction database (http://www.swiss targetprediction.ch/) web server, which predicts the targets of bioactive molecules based on a combination of twodimensional (2D) and 3D similarity measures with known ligands (Daina et al., 2014, 2019; Gfeller et al., 2014), was employed to screen and estimate the putative macromolecular targets of all the compounds from the library. Briefly, these compounds' respective canonical Simplified Molecular Input-Line Entry System (SMILES) structure formats were individually converted using the ChemDraw tool before being imported into the SwissTargetPrediction network database to be queried. After the SMILES structures were uploaded to the database, the species "Homo sapiens" was selected, and a report of probable matched targets data was obtained. Macromolecular targets of interest for further investigations were identified for each compound based on predicted probability, under a criterion of probability >.112.

# 2.3.2 | In silico molecular docking simulation methodology

Docking simulations were conducted with the AutoDock program suite, according to generally established and promulgated protocols (Burley et al., 2018). SMILES structures of ligands marketed for clinical use were retrieved from the PubChem network database (https://pubchem.ncbi.nlm.nih.gov/) (Burley et al., 2018; Trott & Olson, 2010), and these were converted into 3D configuration using OpenBabel, as were the SMILES strings for our synthesized compounds to be tested. Suitable 3D crystallographic structures of each of the protein targets were retrieved from the RCSB Protein Data Bank (PDB) website (https://www.rcsb.org/) (Burley et al., 2018).

The program PyMOL (version 2.3.3) was used to process each raw PDB file data by removing the pre-complexed water molecules, and other standard pre-docking protein preparation procedures in separating the protein and ligand structure from the protein-ligand complex. The separated natural ligand was taken in its bound conformation for use as a native validation control for the docking simulations, and results were also obtained for a known high-affinity ligand (in most instances, ones marketed for clinical use) in comparison to those found for our synthesized ligands. Ligand and de-liganded target structures were then converted to PDBQT files using AutoDock Tools (ADT) incorporated from an opensource software suite (namely, MGL tools 1.5.6; Harris et al., 2008) from the Molecular Graphics Laboratory package from The Scripps Research Institute (http:// autodock.scripps.edu/). During processing (to render the file suitable for initiating a docking simulation), hydrogens were auto-added for nonbonded atoms within the separated (de-liganded) protein structure before conversion to PDBQT format. Most of the tested molecules included at least one bond having restricted rotation, and the initial torsion angle for each ligand was defined as a starting point for each of the docking simulations. While OpenBabel software (v2.2.1) (https://pyrx.sourc eforge.io/) was used for converting the SMILES format of all the ligands to generate their 3D conformations in PDB format, and the program Raccoon was used to establish an initial low-energy conformation (and configuration, where atropisomerism is possible), which was then converted to PDBQT format for use in the docking simulations (Rigsby & Parker, 2016). A grid box (in cartesian coordinates, (11.25-23.00)x-, (11.25-24.06)y-, and (19.12-29.50)z-directions) surrounding the docking site defined according to the particular pre-complexed ligand present in the PDB structure of each target after removing water molecules and hetero atoms for each of the natural ligands in its receptor, with a default grid point spacing of 0.375 Å. The binding affinity was predicted using the freely available graphical user interface (GUI) AutoDock Vina software (v.1.2.0.) (Trott & Olson, 2010), in this case, the Linux OS implementation. After docking simulation with a single computed low-energy starting conformation, other conformations of the docked ligands were obtained, and each ligand with the minimum binding energy and RMSD value was chosen. The ligand and the target complexes were then visualized using PyMOL (Rigsby & Parker, 2016), and BIOVIA Discovery Studio (version 3.5, Dassault Systèmes BIOVIA), for detailed scrutiny. As noted above, known ligands of the studied targets were docked for methodology and procedural validation, and as positive comparators and longitudinal controls for these simulations.

Obtained docking results included estimated binding energies for each ligand: target pair as generated by AutoDock Vina. Results were exported as PDBQT files and were uploaded to PyMOL software to visualize and evaluate the conformation of ligands in the 3D structure data binding models. Binding energies estimated by the software suite were used as docking scores. They were taken as an indication of the potential for a given macromolecular target to be mechanistically involved in, or to contribute to, accounting for, the observed biological activities. Those interactions for which a value  $\leq -8$  (i.e., in principle, with units of Kcal/mol, corresponding to an estimated Kdissoc of  $1.6 \times 10^{-6} \,\mathrm{M} = 1.6 \,\mu\mathrm{M}$ ) were taken as an indication of substantive binding potential, irrespective of the comparable results found for the native or commercial reference ligands.

# 2.3.3 | In silico evaluation of drug-likeness, solubility predictions, physicochemical-based estimations of dermal penetrability, and oral absorbability properties

The SwissADME online server predictor, which provides computed estimates of bioavailability properties, gastrointestinal absorption (GA), druglike nature (druglikeness; DL), and other parameters considered for defining test agent bioactivity, such as the logarithm of the partition coefficient (milog P), the number of hydrogen-bond donors (HBDs), the number of hydrogen-bond acceptors (HBAs), the total topological polar surface area of the compound (TPSA), the number of rotatable bonds (Nrotbs), and aggregate indices of druglikeness, including Lipinski's rule of fives (Pfizer) filter, Ghose filter, Veber (GSK) filter, Egan (Pharmacia) filter, and Muegge (Bayer) filter. These findings were used to assess prospective dermal penetration ability, oral absorbability, and cell membrane penetrability of these compounds (Daina et al., 2019; Gfeller et al., 2014).

# 2.3.4 | Statistical analysis

All statistical analyses were performed using GraphPad Prism Software version 9.1 (GraphPad Prism Inc.) (Roy et al., 2021a, 2021b). All quantitative and grouped data are expressed and presented as means±standard deviation (SD) or ±, standard error of the mean (SEM) from at least three independent experiments. The significance was analyzed by one-way ANOVA, Student's *t*-test or ANOVA with Dunn's multiple comparisons or Bonnferoni's post hoc tests to determine the difference between two or more groups. The following symbols represent the levels of

statistical significance within each analysis: \*p-value < .05, \*\*p-value < .01, \*\*\*p-value < .001 and \*\*\*\*p-value < .001.

## 3 RESULTS AND DISCUSSION

This report represents an initial step toward potentially repurposing a series of molecules previously synthesized in our lab as part of long and tedious efforts to better understand Plasmodium facilparum critical biochemical pathways (Fotie, 2012, 2018). In recent years, our lab has prepared a number of structurally diverse molecules as potential inhibitors of both heme detoxification, and hypoxanthine-guanine-xanthine phosphoribosyltransferase (HGXPRT) pathways in Plasmodium facilparum, with the goal of developing new antimalarial chemotherapeutic agents (Fotie, 2012, 2018, 2019). However, given our current interest in developing and optimizing new scaffolds for their anticancer properties (Chamcheu, et al., 2019; Chamcheu, Roy, et al., 2019; Roy et al., 2021a, 2021b), it seemed auspicious to screen this small library of compounds for their anticancer activities against A375, SK-MEL-28, A431, and SCC-12 skin cancer cell lines. While the synthetic schemes for these compounds are provided in Figure 1 provides a quick insight into the structural diversity of the 35 compounds that displayed relevant attributes through in vitro biological or in silico studies. As such, compounds 1 and 2 are methyl 3,4,5-trimethoxybenzoate derivatives closely related to methyl gallate, and were prepared through electrophilic bromination and nitration, respectively (Fotie et al., 2015). The two 4-cyclohexenylaniline derivatives (3 and 4) were obtained by reacting the corresponding substituted aniline with cyclohexanone in the presence of a catalytic amount of molecular iodine at 160°C, under neat conditions (Fotie et al., 2013), with the same conditions implemented for the preparation of 6- and 8-ethoxy-substituted 2,2,4-tri methyl-1,2-dihydroquinolines 5 and 6, obtained by reacting the corresponding aniline with acetone through Skraup-Doebner-Von-Miller quinoline synthesis (Fotie et al., 2015; Fotie, Kemami Wangun, et al., 2012). Furthermore, under similar conditions, using cyclopentanone instead of acetone, compound 7 was produced, and while reacting a 2,2,4-trimethyl-1,2-dihydroquinoli ne in the presence of either cyclohexanone or cyclopentanone, compounds 8 and 9 were produced, respectively (Fotie et al., 2013; Fotie, Kemami Wangun, et al., 2012). The diphenylamine derivative 11, the only compound from the C-N-linked dimers group to display any useable anticancer properties, was prepared by dimerizing the corresponding aniline derivative via a silver(I) catalyzed direct C-H functionalization (Fotie, Rhodus, et al., 2012). Finally, the largest family of compounds screened during this study was also prepared using silver(I) as a catalyst under reaction conditions similar to those used in the preparation of compound 11 (Berkessa et al., 2016). As such, aniline derivatives were cross-coupled with 2-naphthol (β-naphthol) in a regioselective aerobic oxidative crosscoupling, resulting in a direct C-H functionalization, affording a small array of 2'-aminophenyl-β-napthols (12-16), and a series of 2'-aminobiphenyl-2-ol derivatives (17-35) when using phenols instead of naphtols (Berkessa et al., 2016). However, in contrast to sodium persulfate (Na<sub>2</sub>S<sub>2</sub>O<sub>8</sub>) used as the oxidizing agent in the preparation of 11, which resulted in a C-N coupling reaction, hydrogen peroxide (H<sub>2</sub>O<sub>2</sub>) was used as a substitute, resulted in a C-C coupling (Berkessa et al., 2016). The structures of compounds 12 (CCDC 821630) (Berkessa et al., 2016), 13 (CCDC 1442427) (Berkessa et al., 2016), and 16 (CCDC 1442428) (Berkessa et al., 2016) were unambiguously confirmed by single-crystal x-ray diffraction, with the single-crystal x-ray structures shown as thermal ellipsoid representations (50% probability level) provided in Figure 1, and the related data deposited in the Cambridge database, and copies of these materials can be obtained free of charge from CCDC, 12 Union Road, Cambridge CB2 1EZ, UK, http://www.ccdc.am.ac.uk. The reaction schemes related to the preparation of all these compounds as well as their complete characterization are provided in the Appendix S1.

In an attempt to repurpose the series of molecules described above, these compounds were screened for their antiproliferative and cytotoxic activities against cultured cells of a number of skin cancer cell lines, namely melanoma (A375 and SK-MEL-28) and nonmelanoma (A431 and SCC-12) lineages, using MTT and trypan blue dye exclusion assays as previously reported (Chamcheu, et al., 2019; Chamcheu, Roy, et al., 2019; Roy et al., 2021a, 2021b), with NTERT/1 keratinocytes used as a control. The obtained IC<sub>50</sub> values reflect the concentration of added compound estimated to be capable of reducing the measured viability of the cell population by 50% from the maximal confluency for each of the cell lines, and are summarized in Table 1 for the 35 molecules that displayed any noticeable antiproliferative activity against any of the cell lines. The limited structural diversity for the hit compounds does not allow for a comprehensive structureactivity relationship, but some preliminary observations were made. These compounds appeared to be primarily active against the nonmelanoma A431 and SCC-12 cell lines, with only a handful displaying any appreciable activity against the melanoma A375 and SK-MEL-28 cell lines (Table 1). Among the substituted benzene derivatives, the two substituted methylgallates 1 (IC<sub>50</sub> 8.6  $\mu$ M) and 2 (IC<sub>50</sub> 4.7  $\mu$ M), and the aniline derivative **10** (IC<sub>50</sub> 5.10  $\mu$ M), exhibited low-micromolar activity against the A431 cell line,

FIGURE 1 List of compounds from the library that displayed any useable activity against any of the cell lines used in the in vitro cell culture assays.

while cyclohexenyl anilines 3 and 4 were less active, with all of them being inactive against the other cancer cell lines used in this study.

Nevertheless. N<sup>1</sup>,N<sup>2</sup>-diethyl-N<sup>1</sup>-methoxyphenylphenylenediamine 11 (A431:  $IC_{50} = 5.0 \,\mu\text{M}$ , 12:  $IC_{50} = 2.9 \,\mu\text{M}$ , SK-MEL-28:  $IC_{50} = 4.9 \,\mu\text{M}$ , A375:  $IC_{50} = 6.7 \,\mu\text{M}$ ), obtained by a dimerization of the aniline derivative 10, exhibited reasonable potency across all the four cell lines. Its cell-viability-reducing effect was minimal on the immortalized noncancerous NTERT/1 cells, indicative of better selectivity comparatevely to that of the control drug cisplatin, an agent clinically used in the treatment of an array of human cancers (Almeida & Dos Santos, 2023; Tang et al., 2023; Wang et al., 2023). On the other hand, 1,2-dihydroquinolines **5** (A431:  $IC_{50} = 10 \mu M$ , SK-MEL-28:  $IC_{50} = 12 \mu M$ ), **6** (A431:  $IC_{50} = 10 \mu M$ , SK-MEL-28:  $IC_{50} = 36 \mu M$ ), and **7** (A431:  $IC_{50} = 10 \mu M$ , SK-MEL-28:  $IC_{50} = 17 \,\mu\text{M}$ ) displayed the same level of activity

against the nonmelanoma A431 cell line. Surprisingly, they were also more active against the SK-MEL-28 melanoma cell line than they were against the other nonmelanoma SCC-12 cell line. Yet, they were all inactive against A375, the other melanoma line used in this study. Cycloalkenyl-1,2-dihydro-2,2,4-trimethylquinoline derivatives (8, 9) were less active than the other analogs (5, 6, 7) across all the cell lines. Several 1-(2-aminophenyl)-β-naphthols 2-(2-aminophenyl)-α-naphthol **(16)** 2'-amino-(1,1'-biphenyl)-2-ols (17–35) displayed various level of activity against these cell lines. Many of them exhibited a decent antiproliferative activity against the A431 cell line, notably **12** (IC<sub>50</sub>=10  $\mu$ M), **13** (IC<sub>50</sub>=8.0  $\mu$ M), **15**  $(IC_{50}=8.0 \,\mu\text{M})$ , **17**  $(IC_{50}=6.6 \,\mu\text{M})$ , **19**  $(IC_{50}=8.0 \,\mu\text{M})$ , and 33 (IC<sub>50</sub>=13  $\mu$ M), which were only marginally active or completely inactive against noncancerous immortalized NTERT/1 cells. Compound 13 (A431:  $IC_{50} = 5.0 \,\mu\text{M}$ , SCC-12:  $IC_{50} = 3.3 \,\mu\text{M}$ , SK-MEL-28:  $IC_{50} = 14 \,\mu\text{M}$ , A375:

**TABLE 1** Antiproliferative activity ( $IC_{50}$ ;  $\mu M$ ) of the hit compounds against four human skin cancer cell lines; melanoma (A375 and SK-MEL-28) and nonmelanoma (A431 and SCC-12) cells, with NTERT/1 keratinocytes as a control.

	Nonmelanoma cel	ll lines	Melanoma cell line	es	Normal cell line
Compounds	A431 (IC <sub>50</sub> μM) <sup>a</sup>	SCC-12 (IC <sub>50</sub> μM) <sup>a</sup>	SK-MEL-28 (IC <sub>50</sub> μM) <sup>a</sup>	A375 (IC <sub>50</sub> μM) <sup>a</sup>	NTERT/1 (IC <sub>50</sub> μM) <sup>2</sup>
1	$8.60 \pm 0.55$	$35.5 \pm 1.81$	>40.0	>40.0	NA
2	$4.70 \pm 0.78$	$35.9 \pm 0.85$	>40.0	>40.0	NA
3	$12.8 \pm 1.69$	$31.9 \pm 3.31$	>40.0	>40.0	NA
4	$20.6 \pm 0.74$	$33.3 \pm 0.68$	>40.0	>40.0	>40.0
5	$10.4 \pm 1.34$	$27.9 \pm 1.30$	$12.2 \pm 2.44$	>40.0	>40.0
6	$10.1 \pm 1.89$	>40.0	$36.4 \pm 1.22$	>40.0	>40.0
7	$10.0 \pm 0.91$	$24.6 \pm 3.71$	$17.1 \pm 0.38$	>40.0	NA
8	$14.8 \pm 0.73$	>40.0	>40.0	>40.0	NA
9	$15.2 \pm 3.50$	$34.7 \pm 0.88$	>40.0	>40.0	>40.0
10	$5.10 \pm 1.06$	$31.9 \pm 3.31$	>40.0	>40.0	NA
11	$5.00 \pm 0.80$	$2.90 \pm 0.58$	$4.90 \pm 0.55$	$6.70 \pm 0.47$	$18.0 \pm 1.14$
12	$10.0 \pm 0.76$	$12.9 \pm 1.50$	$29.9 \pm 1.10$	>40.0	NA
13	$5.00 \pm 0.94$	$3.30 \pm 0.58$	$13.8 \pm 0.88$	$17.1 \pm 0.94$	$35.6 \pm 3.45$
14	$17.1 \pm 1.02$	$16.3 \pm 0.28$	>40.0	>40.0	>40.0
15	$8.00 \pm 1.24$	$13.3 \pm 0.27$	$24.8 \pm 1.25$	>40.0	NA
16	$14.0 \pm 0.71$	$32.8 \pm 1.78$	>40.0	>40.0	>40.0
17	$6.60 \pm 0.56$	$23.5 \pm 1.76$	>40.0	>40.0	>40.0
18	$17.5 \pm 2.14$	>40.0	>40.0	>40.0	>40.0
19	$8.00 \pm 2.95$	$18.6 \pm 1.15$	>40.0	>40.0	NA
20	$17.1 \pm 2.40$	$25.3 \pm 1.45$	>40.0	>40.0	>40.0
21	$15.3 \pm 6.12$	>40.0	>40.0	>40.0	>40.0
22	$32.8 \pm 1.55$	$16.5 \pm 0.52$	$31.1 \pm 0.90$	>40.0	>40.0
23	$16.9 \pm 2.21$	>40.0	$32.2 \pm 1.44$	>40.0	>40.0
24	$16.2 \pm 1.15$	$18.3 \pm 1.07$	$39.1 \pm 1.02$	>40.0	>40.0
25	$28.6 \pm 5.04$	$17.1 \pm 1.59$	$17.5 \pm 1.83$	>40.0	NA
26	$22.8 \pm 2.14$	$33.7 \pm 1.45$	>40.0	>40.0	>40.0
27	$24.0 \pm 3.45$	$18.0 \pm 1.41$	$38.6 \pm 1.53$	>40.0	>40.0
28	$30.2 \pm 2.83$	$22.4 \pm 1.49$	$28.6 \pm 2.84$	>40.0	>40.0
29	$33.5 \pm 0.11$	$32.2 \pm 2.93$	>40.0	>40.0	>40.0
30	$20.9 \pm 2.18$	$30.0 \pm 0.79$	>40.0	>40.0	>40.0
31	$23.5 \pm 3.81$	$31.8 \pm 1.97$	>40.0	>40.0	>40.0
32	$38.8 \pm 2.15$	$26.2 \pm 1.26$	>40.0	>40.0	>40.0
33	$12.6 \pm 0.71$	$38.9 \pm 0.09$	>40.0	>40.0	>40.0
34	$21.4 \pm 1.48$	$28.4 \pm 1.79$	>40.0	>40.0	>40.0
35	$22.6 \pm 1.99$	$28.7 \pm 0.21$	>40.0	>40.0	>40.0
Cisplatin <sup>b</sup>	$7.7 \pm 0.34$	$4.4 \pm 0.24$	$14.21 \pm 0.24$	$1.49 \pm 0.44$	$9.1 \pm 1.1$

Note: GraphPad Prism software was used for statistical analyses.

<sup>&</sup>lt;sup>a</sup>Data are expressed as the mean  $\pm$  SD from the dose–response curves of at least six independent experiments performed in sextuplicates; the incubation time for each compound with cells was 48 h; the cytotoxicity was measured by MTT assay;  $IC_{50}$ : compound concentration required to inhibit tumor cell proliferation (assessed as cell viability) by 50%.

 $<sup>^{\</sup>rm b} \text{Cisplatin}$  (a well-known anticancer agent) was used as positive controls.

 $IC_{50} = 17 \mu M$ ) was the most active of the group across all cell lines, with a decent selectivity index when compared to its activity against the noncancerous immortalized NTERT/1 cells.

The substantial divergence in activity across all cell lines between **13** and **12**, differing only by the nature of 5' substituent (ethoxy in the former vs. methyl in the latter) suggests either a beneficial effect of aromatic ring electron enrichment (inductive), or that a one-atom extension of the substituent better fills the potential target binding pocket.

Furthermore, the rotational constraint imposed by the ortho-amino substitution of the 2' aminophenyl substituent in conjunction with the β-naphthol to which they are attached creates the likelihood that each of these compounds might be present as two atropisomers, in not-yet-characterized proportions, which might not be the same for each compound. Such atropisomers would be expected to have disparate target-level affinities and function, confounding the interpretation for this series, including 2-(2-aminophenyl)- $\alpha$ -naphthol (16) and all the 2'-amino-(1,1'-biphenyl)-2-ol derivatives (17-35). In addition, the fact that the presence of a wide array of substituents on the phenol moiety (p-Br (18), p-Cl (19), p-OMe (20), p-Me (21), p-iPr (22), 2,4-diCl (24), or 2,4-diMe (25)) reduced the activity as compared to 17 which bears an unsubstituted phenol, suggests that the electronic features of this latter ring does not substantively participate in charge-transfer type ligand-target interactions, and that the para-position to the phenol is likely remote from any potential target engagement. The variation of the size of the substituent on the nitrogen of the aniline coupling partner beyond a methyl group (26-35) does not seem to have a significant impact on the activity.

While the overall antiproliferative activities exhibited by these lead compounds are not particularly exceptional, it should be pointed out that they are still prominent in many ways, considering that the assays were performed on solid tumor cells. Furthermore, some of the hit compounds exhibited higher potency and better selectivity than cisplatin, a well-known anticancer agent used as a positive control in this study. In fact, as a preemptive attempt to investigate the toxicity of compounds 11 and 13, the PROTOX II web-tool was used where the virtual LD<sub>50</sub> values supported the observed in vitro selectivity of these hits, as compared to the standard control drugs used (Table S1). As can be gleaned from Table S1, compounds 11 and 13 belong to the safer toxicity class 5, whereas the positive control drugs 5-FU appeared in Class 4, and cisplatin in Class 3 with respect to LD<sub>50</sub> prediction class. Cumulatively, these results suggest that the potency and selectivity of these families of compounds can be improved through structure modifications and further structure–activity relationship studies. This requires a better understanding of the drug-like properties and the potential mechanism of action, as well as the identification of the potential drug target for these compounds.

Toward these objectives, a preliminary computeraided ligand-based target prediction technique, known as "target fishing," was undertaken, using a combination of sophisticated similarity searches followed by molecular docking simulations. SwissTargetPrediction software and database allows for the quantification of similarities between compounds by computing a pair-wise comparison of 1D vectors describing molecular structures (Daina et al., 2017, 2019; Gfeller et al., 2014), determines the Tanimoto index between path-based binary fingerprints (FP2) through 2D measurements (Daina et al., 2017, 2019; Gfeller et al., 2014), and evaluates the Manhattan distance similarity between Electroshape 5D (ES5D) float vectors through a 3D assessment (Armstrong et al., 2010, 2011; Daina et al., 2014, 2019; Gfeller et al., 2014), to intuitively validate the "molecular similarity hypothesis," based on the credence that similar molecules engage in-common binding sites to target in-common proteins (Armstrong et al., 2010, 2011). Proceeding in this manner, the software produces a "CombinedScore" index, which, if 0.5 or higher, can be indicative of the fact that these molecules are reasonably likely to share a common protein target (Daina et al., 2017, 2019; Gfeller et al., 2014). It must be clarified that these predictions are only suggestive of the probability for a molecule to interact with a given protein as a target and not an indication of the compound being pharmacologically active in any particular desirable manner. Nevertheless, "target fishing" has proven to be a fast and impressive way to predict the potential protein target(s) in drug discovery, although somewhat limited in accuracy (Armstrong et al., 2010, 2011; Daina et al., 2014, 2019; Gfeller et al., 2014). Accordingly, molecular interaction simulations were carried out to further map out the observed functional profiles of the hit compounds identified through whole-cell in vitro assays, in conjunction with the similarity-based target predictions. Based on the protein targets identified from the similarity studies and for which suitable 3D structures were available, molecular "docking" was utilized to predict the binding potential and to generate docking scores as rough estimates of binding affinity. Figure 2 provides some examples of a binding pose and hydrogen bonding for compounds 11 and 13, shown in the balls and sticks model for receptors Chk1 (A), Clk4 (B), Fyn (C), and Rock2 (D).

Several hit molecules were predicted to interact with substantial affinity only with a select number of enzymes (phosphodiesterases, kinases, proteases, oxidoreductases, erasers of histone acetylation) and ligand-gated ion channels (cf. Tables S2 and S3). It should be specified that

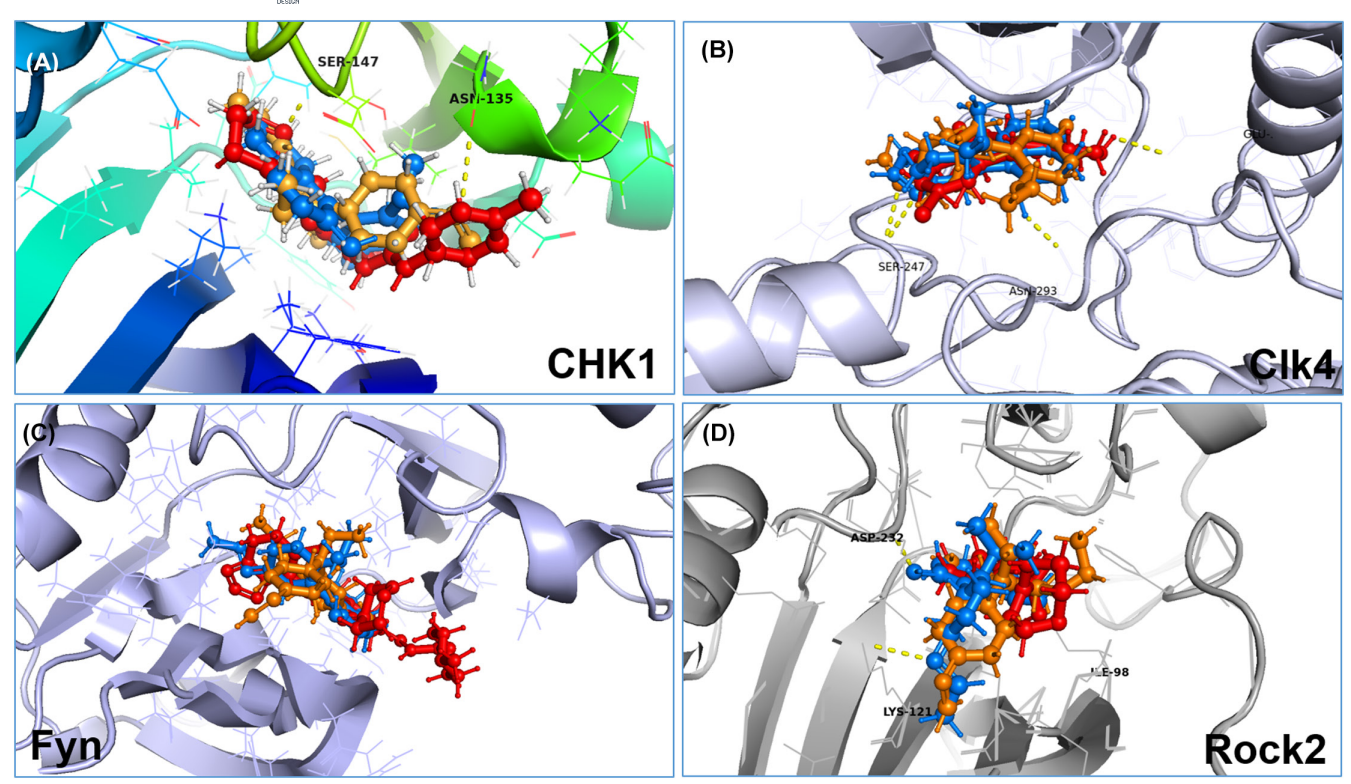


FIGURE 2 Binding pose and hydrogen bonding (yellow dotted line) of each receptor's control compounds, and phenolic 11 and 13 as shown in ball and stick model for receptor Chk1 (A), Clk4 (B), Fyn (C), and Rock2 (D).

many of the identified enzymes, transporters, and receptors have been shown to play essential roles in skin carcinogenesis and cancer progression (Adinolfi et al., 2013; Khasabova et al., 2008; Wohlman et al., 2016).

Taken together with the fact that pharmacological activation of cannabinoid receptors appeared to induce the apoptotic death of tumorigenic epidermal cells without affecting the viability of non-transformed epidermal cells (Casanova et al., 2003), these studies suggest that the suitable interventional modulation of peripheral endocannabinoid signaling could be a promising strategy for the management of some types of cancers. Moreover, lipoxygenases are well known to catalyze the formation of corresponding hydroperoxides from polyunsaturated fatty acids such as linoleic acid and arachidonic acid. They are expressed in immune, epithelial, and tumor cells associated with other physiological conditions, such as skin inflammation, and tumorigenesis (Katikaneni et al., 2020; Spanbroek et al., 1998).

Beyond the target-level potency, the biological activity of small molecules is often influenced to a greater extent by their physicochemical properties, including dermal penetrability. The web tool (Daina et al., 2014, 2019; Gfeller et al., 2014) was used to compute the accords versus violations parameters for these compounds via in silico predictions involving various sets of filter criteria, including the Lipinski (Pfizer) filter (Lipinski et al., 2001), the Ghose

filter (Ghose et al., 1999), the Veber (GSK) filter (Veber et al., 2002), the Egan (Pharmacia) filter (Egan et al., 2000), and Muegge (Bayer) filter (Muegge et al., 2001). The obtained results (Table 2) indicate that the physicochemical characteristics of all the hit compounds are well within the defined parameters for a good drug candidate. More importantly, the bioavailability score of about 0.55 obtained for all these compounds satisfies Lipinski's rule for a neutral compound, indicative of their suitability for absorption through oral ingestion (Lipinski et al., 2001), and provides a reasonable basis for lead optimization endeavors and further structure–activity relationship studies.

Pan-assay interference compounds (PAINS) are promiscuous molecules defined by common substructural motifs that encode for an increased chance of any member registering as a hit in any given assay, almost independently of platform and technology (Baell & Holloway, 2010; Baell & Nissink, 2018; Lagorce et al., 2015; Saubern et al., 2011). These interferences arise through various mechanisms including, reactivity with biological and bioassay nucleophiles such as thiols and amines, photoreactivity with any protein functionality, metal chelation that can interfere with proteins or through bringing in heavy metal contaminants, redox cycling and redox activity, physicochemical interference such as micelle formation, or possess photochromic properties that might interfere with typically used assay signaling such as absorption and fluorescence

13 of 2

(Continues)

TABLE 2 Physicochemical and biopharmaceutical properties of the hit compounds.

	Lipophilicity							Drugliken	ass (num	Druglikeness (number of violations)	ions)		Bioavailability	oility		
Σ	MW (g/mol)	IlogP	XlogP3	WlogP	MlogP	Silicos-IT logP	Consensus logP	Lipinski	Ghose	Veber	Egan	Muegge	Log K <sub>p</sub> (cm/s)	F	ESOL	# PAIN alerts
8	384.018	3.18	3.07	3.02	2.17	3.23	2.93	0	0	0	0	0	-6.46	0.55	-4.07	0
2	271.223	2.23	1.52	1.41	-0.11	-0.26	96.0	0	0	0	0	0	-6.88	0.55	-2.32	0
7	201.307	3.00	4.65	3.71	3.38	3.23	3.60	0	0	0	0	1	-4.23	0.55	-4.18	1
Cl	235.752	3.21	4.62	4.54	3.91	4.29	4.11	0	0	0	0	1	-4.46	0.55	-4.29	0
(1	217.307	3.01	3.11	3.12	2.73	3.32	3.06	0	0	0	0	0	-5.42	0.55	-3.29	0
(1	203.280	2.72	2.74	2.73	2.46	2.96	2.72	0	0	0	0	0	-5.59	0.55	-3.06	0
(.,	335.482	4.20	4.78	5.76	4.74	5.82	5.06	1	1	0	0	0	-4.95	0.55	-4.91	1
(1	297.434	4.04	4.83	5.08	4.09	5.09	4.62	0	0	0	0	0	-4.69	0.55	-4.73	1
(.,	305.456	4.21	5.13	5.86	5.10	5.89	5.24	1	1	0	0	2	-4.52	0.55	-5.03	0
	151.206	2.24	1.60	1.94	1.80	1.83	1.88	0	1	0	0	1	60.9-	0.55	-1.99	1
(.,	300.395	3.56	4.26	4.10	3.01	3.17	3.62	0	0	0	0	0	-5.11	0.55	-4.33	1
(4	277.360	3.18	4.93	4.59	3.97	4.20	4.17	0	0	0	0	0	-4.49	0.55	-5.10	0
(.,	307.386	3.43	4.90	4.68	3.59	4.11	4.14	0	0	0	0	0	-4.70	0.55	-5.08	1
(1)	383.482	4.16	6.40	6.10	4.65	5.59	5.38	1	1	0	1	1	-4.10	0.55	-6.41	1
m	347.450	4.14	5.78	5.62	4.17	5.11	4.96	1	1	0	0	1	-4.32	0.55	-5.69	1
7	277.360	3.27	4.93	4.59	3.97	4.20	4.19	0	0	0	0	0	-4.49	0.55	-5.10	0
7	257.328	3.17	3.65	3.52	2.84	3.03	3.24	0	0	0	0	0	-5.28	0.55	-3.94	1
m	336.224	3.62	4.34	4.29	3.47	3.70	3.88	0	0	0	0	0	-5.27	0.55	-4.84	1
CI	291.773	3.51	4.28	4.18	3.35	3.66	3.88	0	0	0	0	0	-5.04	0.55	-4.53	1
(1	287.354	3.68	3.63	3.53	2.50	3.08	3.28	0	0	0	0	0	-5.48	0.55	-4.00	1
(4	271.354	3.35	4.02	3.83	3.09	3.54	3.57	0	0	0	0	0	-5.10	0.55	-4.23	1
(4	299.407	3.70	4.78	4.65	3.56	4.15	4.17	0	0	0	0	0	-4.73	0.55	-4.78	1
. 4	291.773	3.53	4.28	4.18	3.35	3.66	3.80	0	0	0	0	0	-5.04	0.55	-4.53	1
( - 1	326.218	3.30	4.77	4.83	3.86	4.31	4.21	0	0	0	0	0	-4.90	0.55	-5.03	1
(4	285.381	3.43	4.38	4.14	3.32	4.06	3.87	0	0	0	0	0	-4.93	0.55	-4.53	DESIGN
	285.381	3.75	4.55	4.30	3.32	3.80	3.95	0	0	0	0	0	-4.81	0.55	-4.50	1
(.,	364.277	3.41	5.24	5.07	3.94	4.48	4.43	0	0	0	0	1	-4.80	0.55	-5.41	1
(4	299.407	3.56	4.98	4.55	3.56	4.02	4.13	0	0	0	0	0	-4.59	0.55	-4.84	1
(.,	378.303	4.16	2.68	5.31	4.16	4.70	4.80	0	0	0	0	1	-4.57	0.55	-5.75	1
(.,	364.277	3.84	5.14	5.07	3.94	4.31	4.46	0	0	0	0	1	-4.87	0.55	-5.41	1
	333.424	3.70	5.15	4.94	3.99	4.54	4.46	0	0	0	0	1	-4.68	0.55	-5.29	1

# PAIN alerts -5.64ESOL -5.310.55 0.55 Bioavailability Log Kp (cm/s) -4.67 -4.92-4.64-4.62Muegge Druglikeness (number of violations) 0 0 Veber 0 0 0 Ghose 0 0 Lipinski 0 0 Consensus logP 5.05 4.84 4.27 4.46 Silicos-IT 5.22 4.19 4.87 3.56 4.16 3.94 WlogP 5.70 4.69 5.46 5.07 5.84 4.91 5.61 5.08 3.92 3.75 3.99 4.08 Lipophilicity MW (g/mol) 364.277 412.320 299.407 378.303 33 34 35

TABLE 2 (Continued)

Note: Molecular weight (MW), LogP values (an indicator of lipophilicity), aqueous solubility parameters (ESOL) an indicator of skin permeation (Log  $K_p$ ), bioavailability score (F), and number of pan-assay interference (PAINS) alerts.

(Baell & Holloway, 2010; Baell & Nissink, 2018; Lagorce et al., 2015; Saubern et al., 2011).

However, it is essential to note that identifying individual compounds with a PAINS substructure does not necessarily imply that the molecule is promiscuous or will invariably exhibit broad-spectrum interference. Approximately 5% of FDA-approved drugs contain PAINS-recognized substructures and have exhibited multiple PAINS alerts (Baell & Holloway, 2010; Baell & Nissink, 2018; Lagorce et al., 2015; Saubern et al., 2011). Therefore, these PAINS filters and alerts, much like Lipinski's rule of five, serve as guiding principles rather than strict rules (Baell & Holloway, 2010; Baell & Nissink, 2018; Lagorce et al., 2015; Saubern et al., 2011).

Consequently, all the molecules involved in this study were subjected to SwissADME PAINS filters, and the number of alerts for each compound is reported in Table 2. Eight of these compounds (1, 2, 4, 5, 6, 9, 12, and 16) exhibited no PAINS alerts, while the remaining compounds each showed one PAINS alert, likely due to the potential redox cycling properties of phenol and aniline substructures. However, this does not necessarily imply that these molecules are inherently promiscuous or guaranteed to cause interference in the assays reported in this study. In fact, as the compounds exhibiting this single alert share a similar substructure, while also displaying a widely different level of activity in the cell inhibition assay, it is highly unlikely that the observed antiproliferative properties result from a PAINS interference attributable to the shared subunit.

As the primary objective of this exercise is not only to identify hit compounds from a small library of molecules with unsuspected biological activity, but also to frame their pharmacological profile for further optimization through a rationale design and synthesis of analogs, more studies were initiated to determine the potential antiproliferative mechanism of action, and the potential drug target(s) for the two most active hit compounds. As such, the effects of compounds 11 and 13 on wound healing, colony formation, and on the apoptotic pathways were investigated. Using scratch wound assay, the abilities of compounds 11 and 13 to restrict the growth or migration of SCC-12 and SK-MEL-28 cells into cell-free areas produced by scratchwounding were assessed. Both compounds significantly inhibited cell migration into the scratched wound areas relative to the untreated control, in a dose-dependent manner after a 48 h incubation (Figure 3).

While exploring the long-term (2-week treatment in 2D culture) impacts of different concentrations (0,  $\frac{1}{2}IC_{50}$ ,  $IC_{50}$ , and  $\frac{1}{2}IC_{50}$ ;  $IC_{50}$  values obtained from the proliferation studies with cells of the same line) of compounds **11** and **13** on colony formation, these compounds appeared to significantly reduce the number of colonies formed

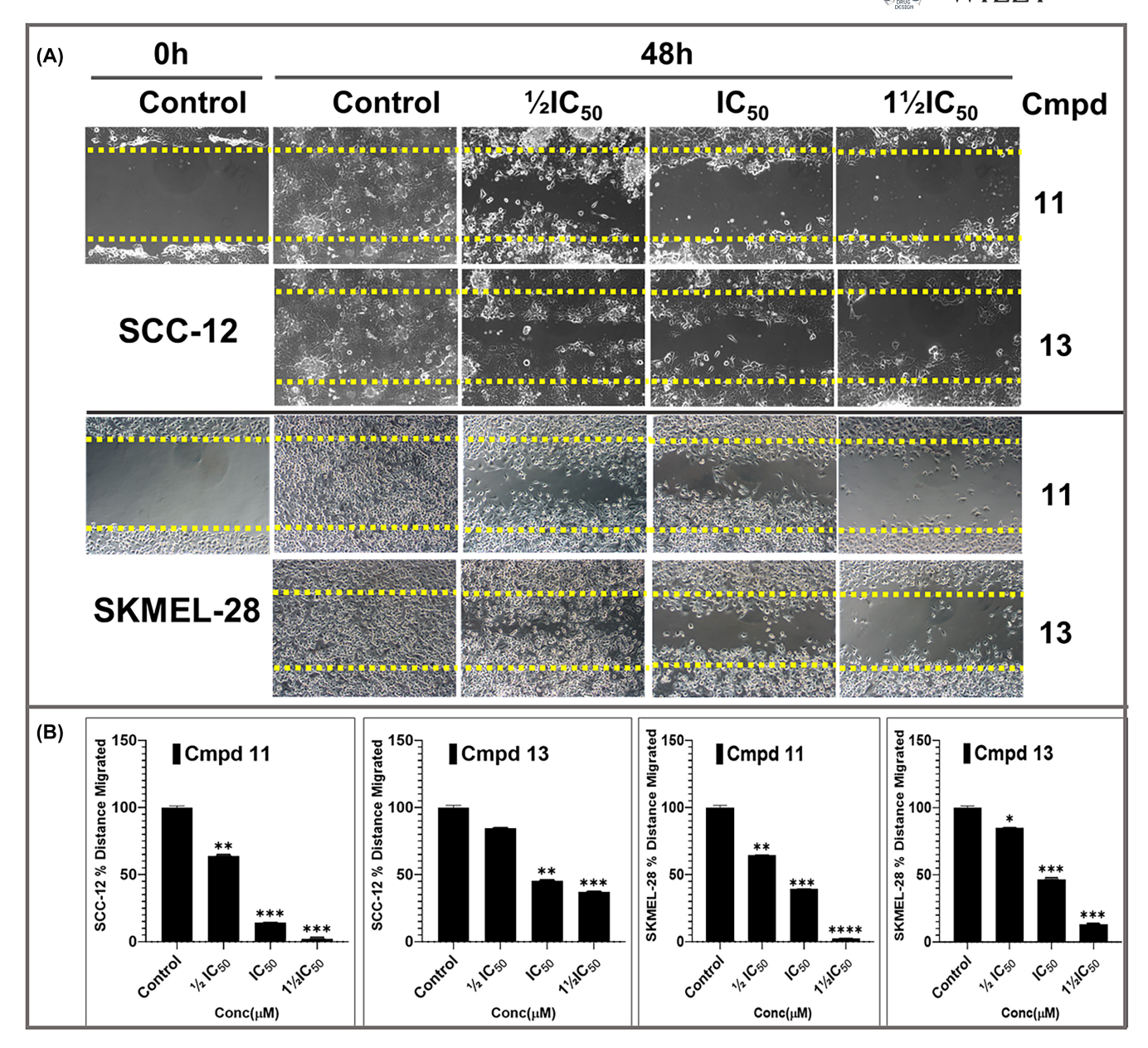


FIGURE 3 The relatively potent hit compounds **11** and **13**, dose-dependently  $(0, \frac{1}{2}IC_{50}, IC_{50}, and \frac{1}{2}IC_{50}, IC_{50}$  values obtained from the proliferation studies with cells of the same line,  $\mu$ M), inhibited the in vitro migration of SCC-12 (A; top panel) and SK-MEL-28 (A; bottom panel) cells into the cell-free wounded areas of a confluent cell monolayer scratched wound. Dose-dependent suppression of wound closure by compounds **11** and **13** with cultured SCC-12 and SK-MEL-28 cells (B) shows test compounds' effect in limiting the migration of cells into the inflicted in vitro wounds. The bar graphs (B) represent the mean  $\pm$  SD of scratched wound area values after 48 h expressed as a percentage at 0 h untreated control from three independent experiments conducted in triplicates. Statistical significance was assessed using one-way ANOVA and Dunn's multiple comparison tests; p < .05 (\*), p < .01 (\*\*\*), p < .001 (\*\*\*) and p < .0001 (\*\*\*\*) are indicated, and were all considered significant.

in both SCC-12 and SKMEL-28 cells in a concentration-dependent manner (Figure 4A,B), in comparisons to the corresponding untreated control groups (Figure 4C-F).

Despite the structural differences between 11 and 13, both compounds exhibited relatively strong abilities to decrease cell viability, cell migration, and colony formation. In an attempt to identify attributable molecular mechanisms for each of these two compounds, their apoptotic effects on SCC-12 and SK-MEL-28 cancer cell lines were

explored. Consequently, the effects of **11** and **13** on cellular cytoskeleton (actin staining) and nuclear morphology (DAPI staining) Figure 5A,B (control; c and ca, and drug-treated; g-k and ga-ka), as well as on the activation of proapoptotic caspase-3, were assessed by comparing apoptotic cell fractions and caspase-3 cleavage to untreated groups via an immunofluorescent microscopy analysis. The nuclei of SCC-12 and SK-MEL-28 cells treated with either **11** or **13** exhibited morphologies characteristic of

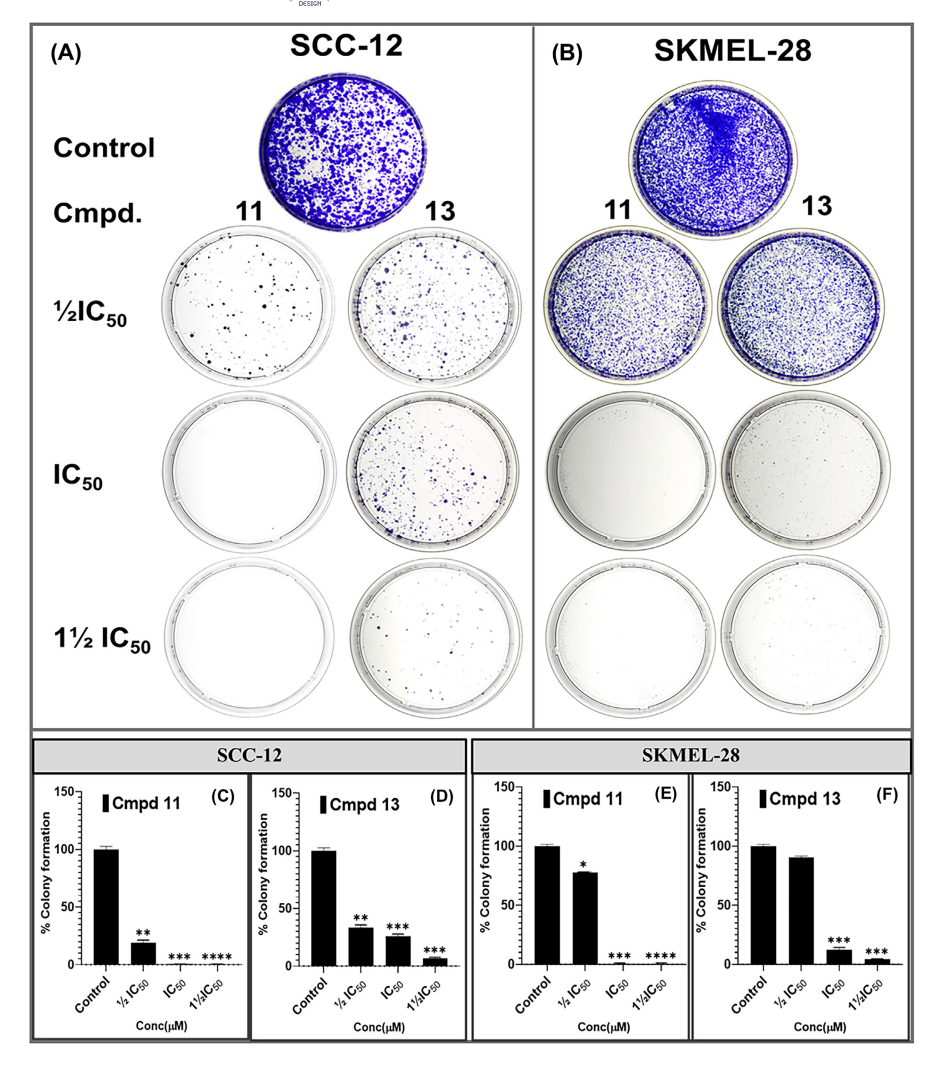


FIGURE 4 Compounds 11 and 13 significantly inhibit colony formation potentials in SCC-12 (A) and SK-MEL-28 (B) cells cultured in monolayers after 14 days when control cells became confluent. The percentage decrease in colony formation is seen to be dose-dependent (0, 1/2IC50, IC50, and 11/2IC50, IC50 values obtained from the proliferation studies with cells of the same line; µM), and was comparable for SCC-12 (C, D) and SK-MEL-28 (E, F) cells. The data expressed in the bar graphs represent the mean  $\pm$  SD of colonies analyzed for compounds 11- and 13-treated groups, expressed as a percentage of the colony number for the untreated control group. Data are from three independent experiments, performed in quadruplicate. Statistical significance was assessed using one-way ANOVA and Dunn's multiple comparison tests; p < .05 (\*), p < .01(\*\*), p < .001 (\*\*\*), and p < .0001 (\*\*\*\*), as indicated, and were all considered significant.

fragmented chromatin, with punctate apoptotic nuclei, in a dose-dependent manner (data not shown). Compared to untreated SCC-12 cells (Figure 5A(a) and B(aa)), which presented a well-organized actin filament radiating across the cell cytoskeleton and extending to the lamellipodia, the drug-treated cells showed disoriented and diminished actin filament cytoskeleton. These effects were dose-dependent for both compounds 11 (Figure 5A(e-i), red) and 13 (Figure 5B(ea-ia), red) on the SCC-12 cell line.

As shown in Figure 6, similar potency was observed for **11** (Figure 6A(e-i), red) and **13** (Figure 6B(ea-ia), red) on the SK-MEL-28 cell line. With regards to the activation of proapoptotic caspase-3, untreated SCC-12 cells showed a regular staining pattern of procaspase-3 (Figure 5A(b) and B(ba), green), while treatment with either compound dose-dependently activated caspase-3 and induced its translocation into the nucleus, as evidenced by the punctuated active caspase-3 immunofluorescence staining detected in the nuclei observed in cells treated with **11** (Figure 5A(f and j) and **13** (Figure 5B(fa and ja). The punctuated caspase-3 staining was colocalized with the nuclear actin staining (Figure 5A (h and i) for **11** and Figure 5B

(ha and ia) for **13**, cyan), and along with their impacts on caspase-3 activation status, compounds **11** (Figure 6A(f and j)) and **13** (Figure 6B(fa and ja)) also exhibited corresponding dose-dependent effects on the actin cytoskeleton, which also served for the localization (cyan yellow) of the actin (red), nucleus (DAPI), and pro and active caspase-3 immunostaining (green) (see Figures 5 and 6).

The cysteinyl aspartate-specific protease family of apoptotic caspases, classified as initiators (caspases 8, 9, and 10) and executioners (caspases 3, 6, and 7), are often targeted for anticancer treatment, including skin tumor treatment (Boice & Bouchier-Hayes, 2020; Dabrowska et al., 2016; Pisani et al., 2020). Using both the immuno-fluorescence microscopy (Figures 5 and 6) and western blot analyses (Figures 7 and 8) of SCC-12 (nonmelanoma) and SK-MEL-28 (melanoma) cell lines, the effects of compounds 11 and 13 on the intrinsic and extrinsic apoptosis pathways were investigated by analyzing the protein expression levels of several key apoptosis-related markers. The assessed markers included an executioner, namely pro- and cleaved (activated) forms of caspase 3 (cf. Figures 5 and 6; green), and an initiator (pro- and cleaved

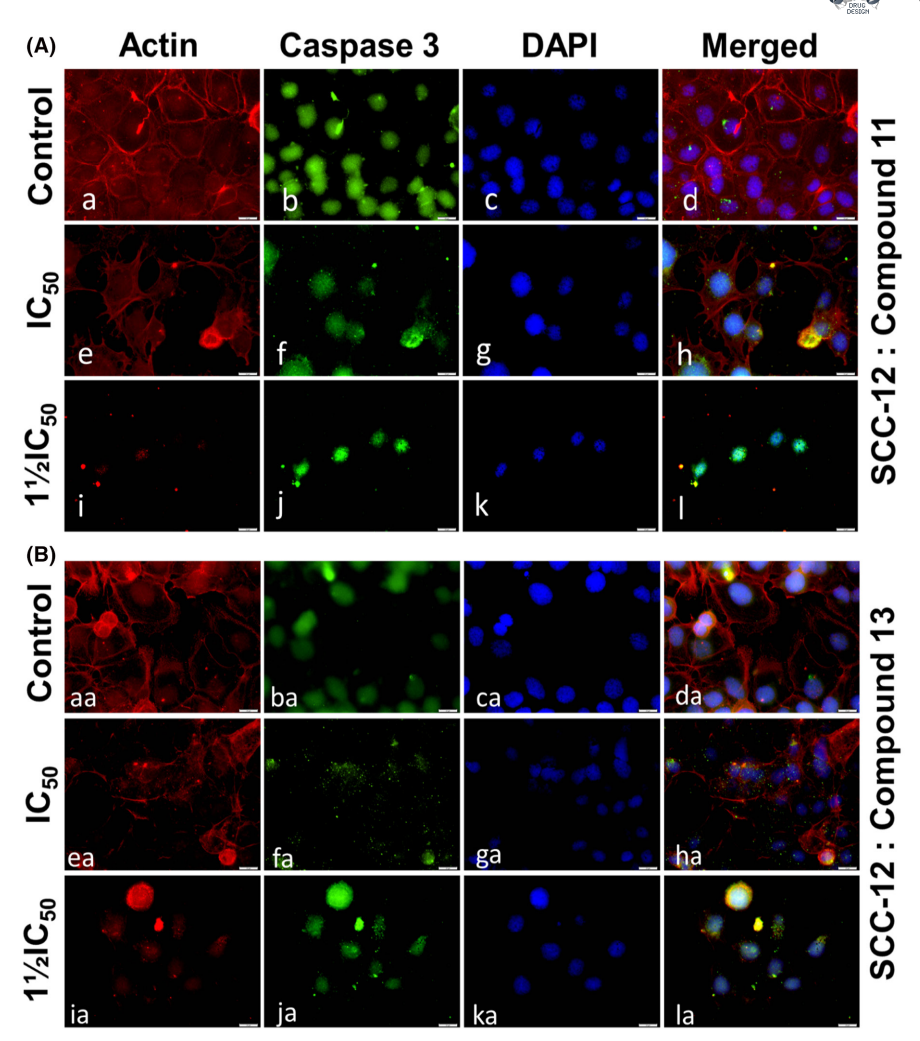


FIGURE 5 Compounds 11 and 13 dose-dependently altered the actin cytoskeleton cell morphology and activated pro-apoptotic caspase-3 translocation into the nucleus of cells of the SCC-12 nonmelanoma skin cancer line. Immunofluorescent micrographs analyses indicate that compounds 11 (A; e-l) and 13 (B; ea-la), as compared to untreated controls (for 11 (a-d) and 13 (aa-da)), morphologically distorted the actin cytoskeleton as well as decreased the actin expression levels (red) in monolayer cultures of SCC-12 cells in a dose-dependent manner (0,  $\frac{1}{2}$ IC<sub>50</sub>, IC<sub>50</sub>, and  $\frac{1}{2}$ IC<sub>50</sub>;  $\mu$ M; red; a, e, i and aa, ae, ai, respectively). Similarly, 11 (A) and 13 (B) prompted activation (green; b, f, j and ba, fa, ja) and translocation of procaspase 3 (green) into the nucleus (DAPI, blue) after treatment (colocalization, cyan) as shown (c, g, k and ca, ga, ka). Photomicrographs delineate the colocalization of actin and active caspase-3 in the nucleus (see h, I and ha, la) upon 11 and 13 treatments, respectively. Images were obtained after 48 h of incubation for SCC-12 cells with or without the test compound, and were analyzed as described in the Section 2.

caspase-9), as well as cleaved PARP, evaluated by western blot analysis. In addition to the elevated levels of cleaved caspase-3 observed by immunofluorescence (Figures 5 and 6), treatment of SCC-12 and SK-MEL-28 cells with either **11** or **13** resulted in significant activation of apoptosis, as evidenced by the increased activation of caspase-9, and of PARP cleavage (Figure 7).

The expression levels of cleaved caspase-9 and cleaved PARP increased in a concentration-dependent manner compared to untreated controls. Furthermore, expression changes occurred for important Bcl-2-family proteins that regulate the induction of the mitochondrial pathway of apoptosis, specifically Bax (proapoptotic) and Bcl-2 (antiapoptotic) (Lopez et al., 2022; Ozoran et al., 2022;

Pisani et al., 2020; Watson et al., 1999), as well as PIM3, another apoptosis-related marker, upon treatment of SCC-12 and SK-MEL-28 cells with 11 or 13, in comparison with untreated controls. Treatment of both SCC-12 and SK-MEL-28 cells with 11 and 13 significantly and dose-dependently increased the protein expression level of Bax while decreasing the expression levels of Bcl-2 and PIM3 compared to the untreated controls (Figure 8). Treatment with either of the two compounds resulted in a concentration-dependent increase in the Bax/Bcl-2 ratio, further endorsing the finding that 11 and 13 can induce the apoptosis of skin cancer cells, here exemplified with SCC-12 and SK-MEL-28 nonmelanoma and melanoma skin cancer cell lines, respectively, through the intrinsic

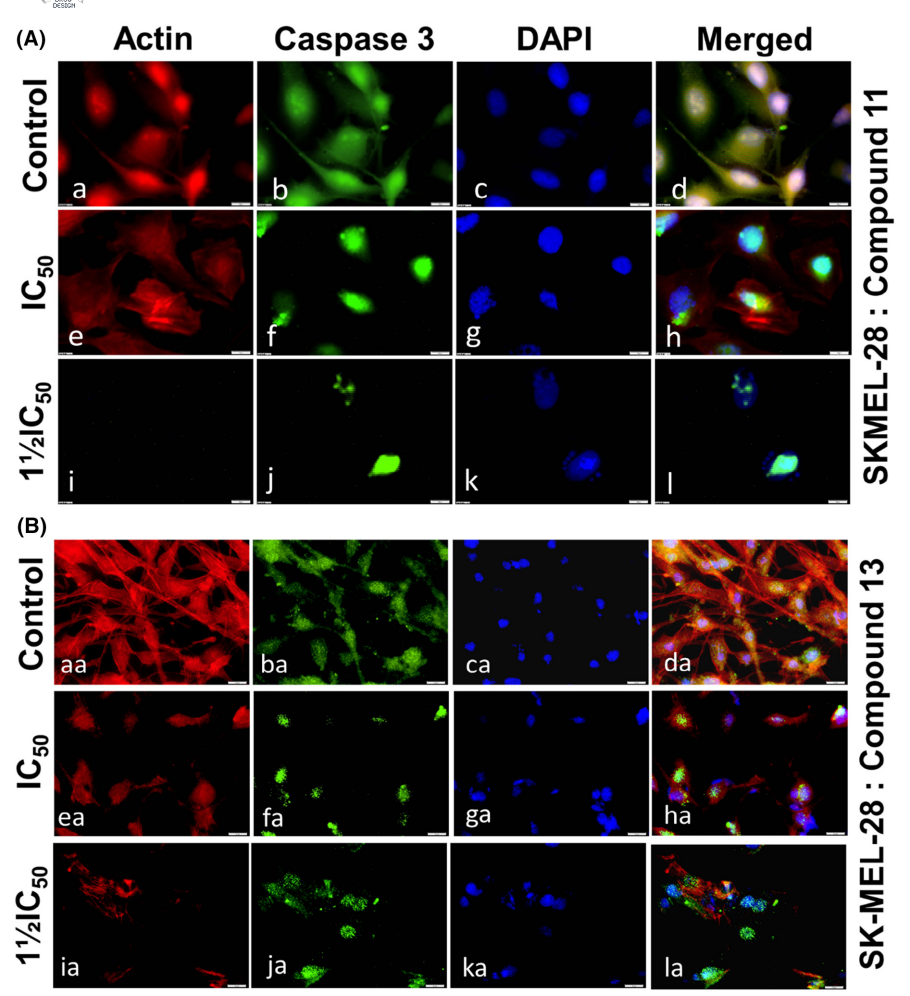


FIGURE 6 Compounds 11 and 13 dose-dependently altered the actin cytoskeleton cell morphology and activated pro-apoptotic caspase-3 expression into the nucleus of cells of the SK-MEL-28 cutaneous melanoma cancer cell line. Immunofluorescent micrographs analyses indicate that compound 11 (A; e–l) and 13 (B; ea–la) by comparison to untreated controls (11 (a–d) and 13 (aa–da)), morphologically distorted the actin cytoskeleton as well as decreased the actin expression levels (red) in monolayer cultures of SK-MEL-28 in a dose-dependent manner (0,  $\frac{1}{2}$ IC<sub>50</sub>, and  $\frac{1}{2}$ IC<sub>50</sub>, and  $\frac{1}{2}$ IC<sub>50</sub>, and aa, ae, ai, respectively). Similarly, 11 (A) and 13 (B) prompted activation (green; b, f, j and ba, fa, ja) and translocation of pro-caspase 3 into the nucleus (DAPI, blue) after treatment (colocalization, cyan yellow) as shown (c, g, k and ca, ga, ka). Photomicrographs delineate the colocalization of actin and active caspase-3 (green) in the nucleus (see h, I and ha, la) upon compounds 11 and 13 treatments, respectively. Images were obtained after 48 h incubation of SK-MEL-28 cells with or without test compounds, and were analyzed as described in the Section 2.

mitochondrial apoptotic pathway, leading to the pronounced activation of PARP cleavage.

It is well documented that uncontrolled cell proliferation and aberrant differentiation, which are the hall-marks of cancers including melanoma and nonmelanoma skin cancers (Enane et al., 2018; Shirakawa et al., 2021; Wiechec et al., 2021) are associated with dysregulated signaling pathways, such as the MAPK/ERK and PI3K/AKT pathways (Acevedo-Diaz et al., 2022; Dong et al., 2021; Luo et al., 2022), and have been therapeutically targeted in several advanced melanoma clinical trials using a wide range of inhibitors (Carvajal et al., 2022; DePalo et al., 2022; Kakish et al., 2022). Furthermore, the levels of phosphorylated p90RSK (Ser380), Akt (Ser473), p44/42-MAPK

(ERK1/2; Thr202/Tyr20), and ribosomal protein S6 (Ser235/236) were significantly suppressed in SCC-12 and SK-MEL-28 cells treated with either compound **11** or **13**, as compared to the untreated controls. Additionally, the treatments of SCC-12 and SK-MEL-28 with escalating concentrations of **11** or **13** (0, IC<sub>50</sub> and  $1\frac{1}{2}$ IC<sub>50</sub>; values for IC<sub>50</sub> from the cell proliferation experiments) for 48 h resulted in a significant reduction in the levels of activated (phosphorylated) AKT, MAPK, and mTOR signaling pathways when compared to untreated controls, as indicated by the western blot analyses (Figure 9).

Considering the binding affinity of compounds **11** and **13** toward a number of kinases, proteases, oxidoreductases and erasers, as well as the interactions observed during

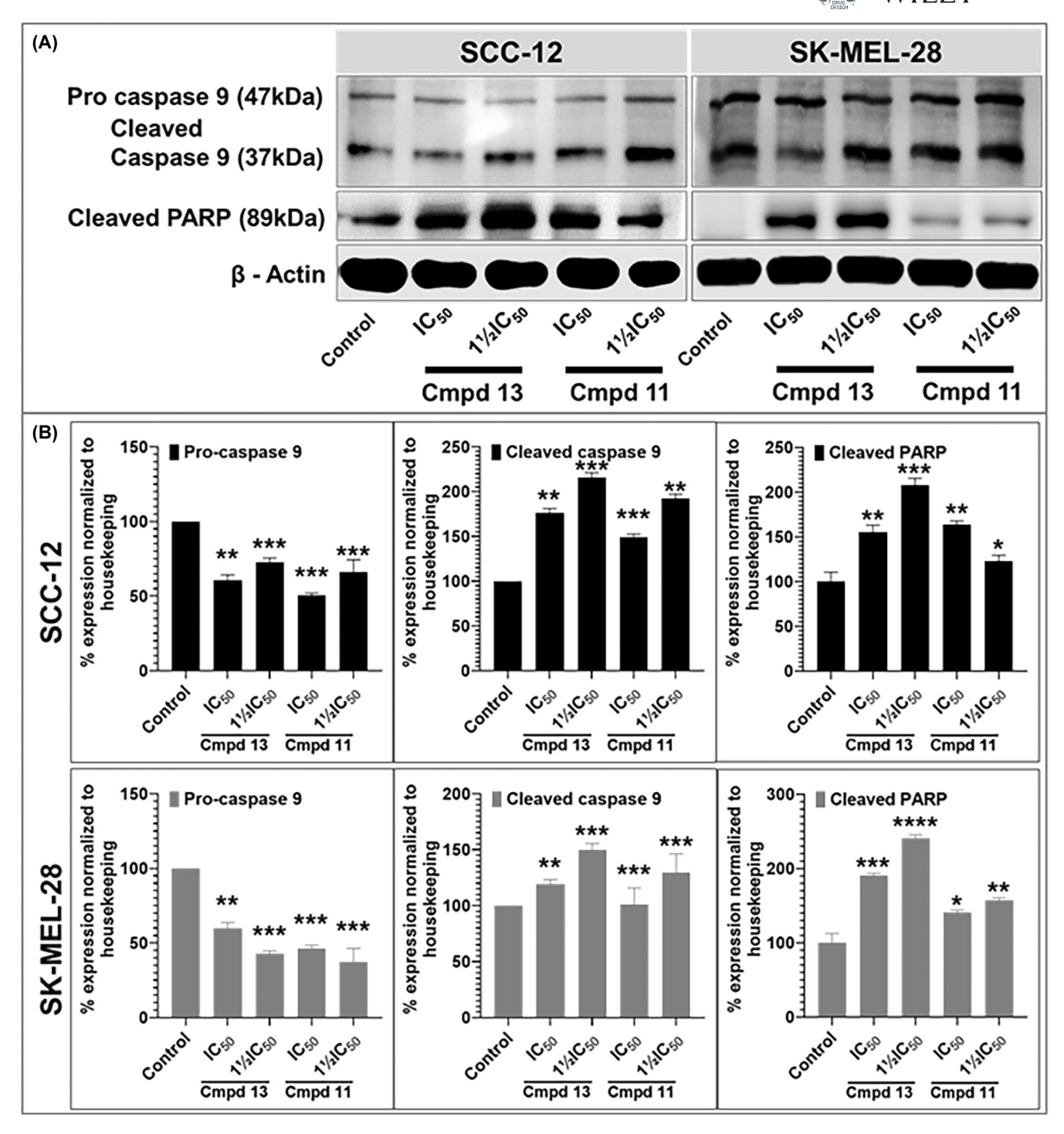


FIGURE 7 Compounds 11 and 13 induce apoptosis by activating the extrinsic and intrinsic apoptotic pathway caspases in cutaneous melanoma (SK-MEL-28) and nonmelanoma cancer cells (SCC-12). (A) The blots show a dose-dependent effect (0, ½IC<sub>50</sub>, IC<sub>50</sub> and  $1½IC_{50}$ ; μM), IC<sub>50</sub> values obtained from the proliferation studies with cells of the same line) on protein expression levels of markers of apoptosis, including pro- and-cleaved caspase 9 and cleaved PARP after 48 h of treatment. (B) The data shown are representative immunoblots from three independent experiments with similar results. β-actin served as a loading control to confirm the loading uniformity. The bar graphs normalized the actual protein optical density values against those for loading control. The resulting values are presented as a percentage versus ratios for untreated control (mean ± SD of relative quantitative density ratios). Statistical significance was assessed using one-way ANOVA and Bonferoni's multiple comparison tests; p < .01 (\*\*\*), p < .001 (\*\*\*\*) and p < .0001 (\*\*\*\*\*) are indicated, all considered to be statistically significant.

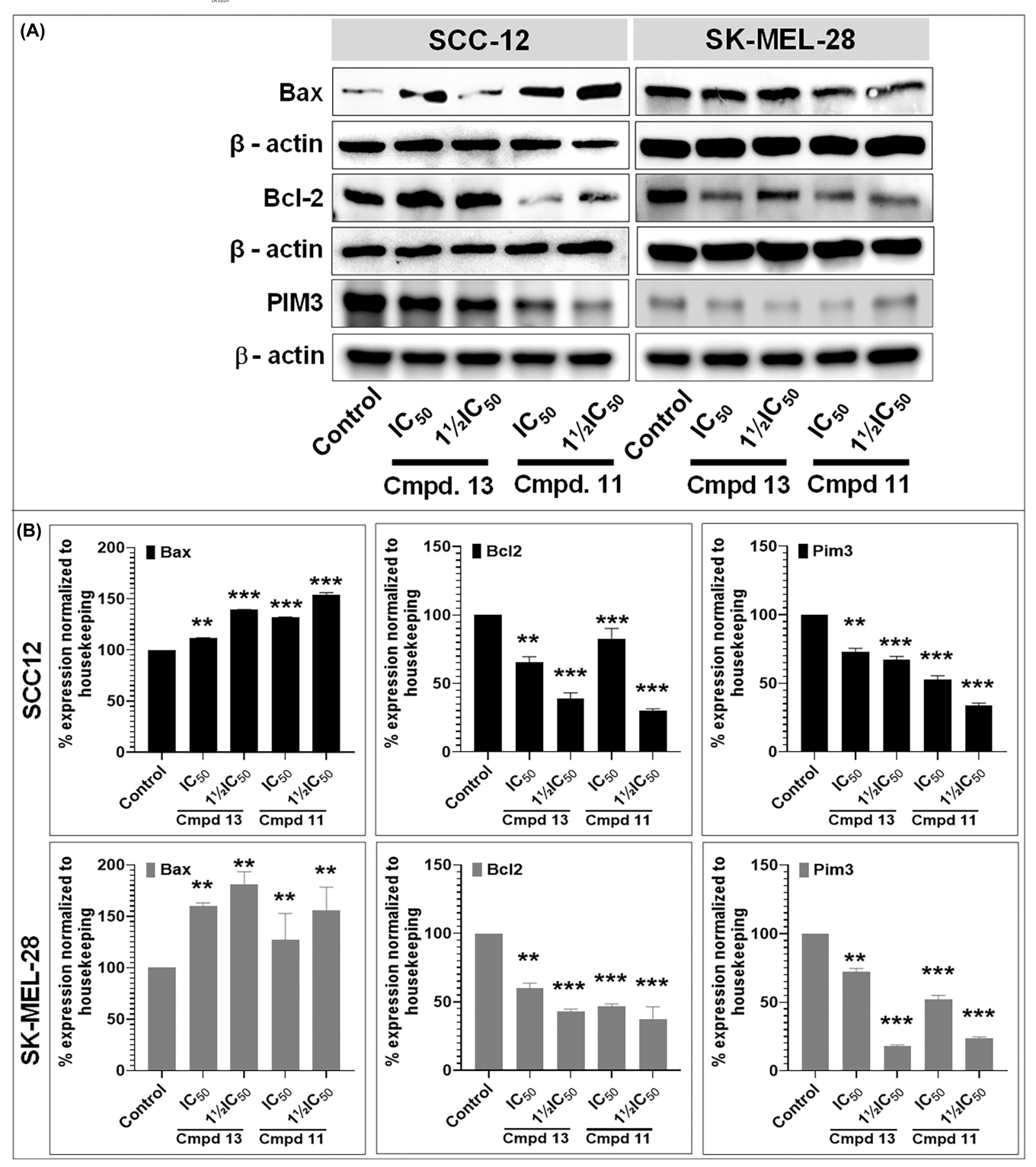


FIGURE 8 Compounds 11 and 13 induce apoptosis by activating the extrinsic and intrinsic apoptotic pathways in cutaneous melanoma (SK-MEL-28) and nonmelanoma (SCC-12) cancer cells. (A) Western blots show a dose-dependent effect  $(0, \frac{1}{2}IC_{50}, IC_{50}, and \frac{1}{2}IC_{50}; \mu M$ , IC<sub>50</sub> values obtained from the proliferation studies with cells of the same line) on protein markers of apoptosis, including Bax, Bcl-2, and PIM3, after 48 h of treatment. (B) The data shown are representative immunoblots from three independent experiments. β-Actin was used as a loading control to confirm loading uniformity. The actual protein optical density values for bar graphs were normalized against those for loading control. The resulting values are presented as a percentage vs. ratios for untreated control (mean ± SD of relative quantitative density ratios). Statistical significance was assessed using one-way ANOVA and Bonferroni's multiple comparison tests; p < .01 (\*\*) and p < .001 (\*\*\*) were considered to be statistically significant.

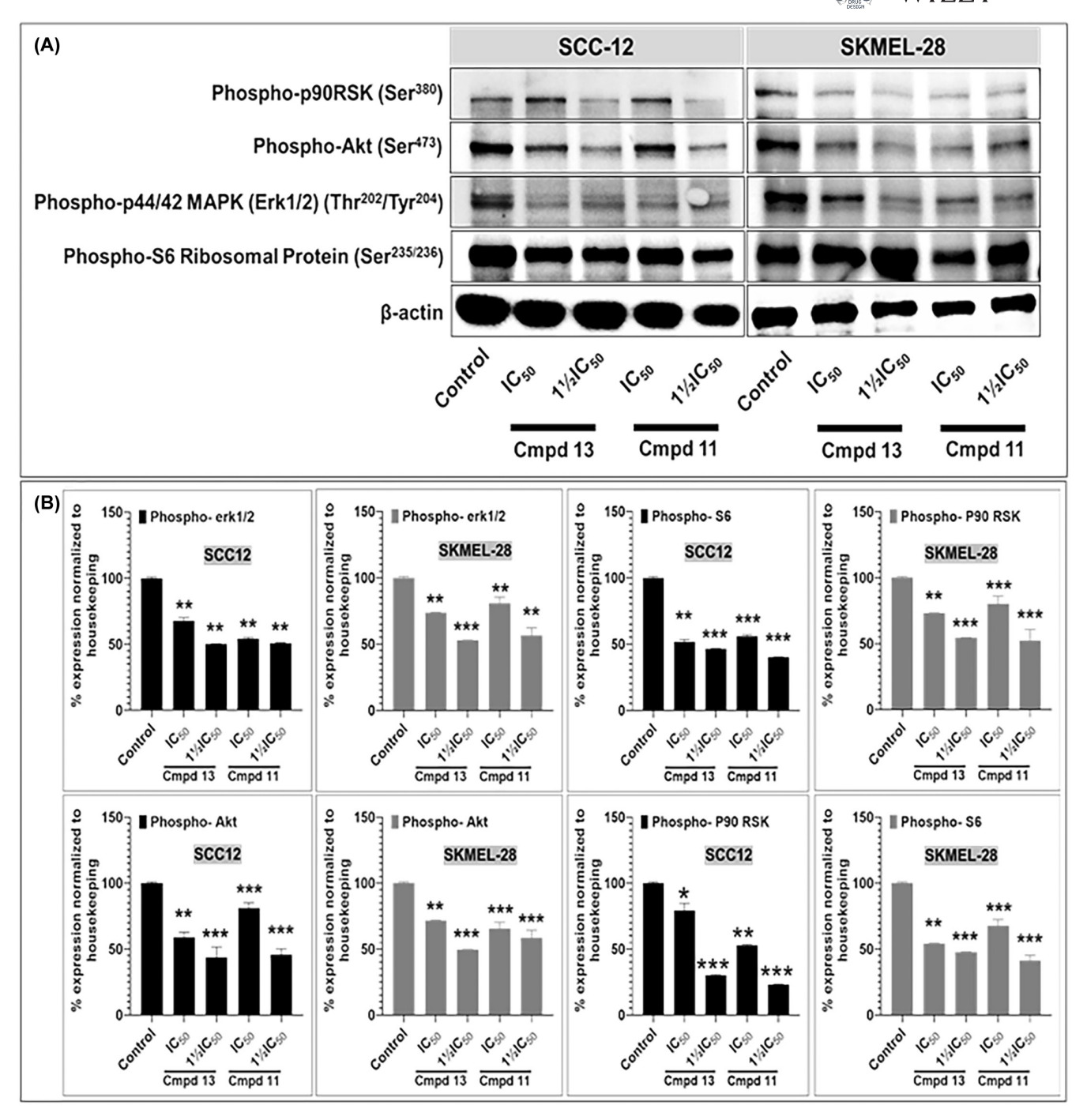


FIGURE 9 Compounds 11 and 13 can inhibit activation of the AKT/mTOR and MAPK pathways, as indicated by the markers phosphorylated p90RSK (Ser380), phosphorylated AKT (Ser473), phosphorylated p44/42 MAPK (Erk1/2) (Thr202/Tyr204), and phosphorylated S6 Ribosomal Protein (Ser235/236) in cutaneous melanoma (SK-MEL-28) and nonmelanoma (SCC-12) skin cancer cells. (A) Western blots show a dose-dependent effect (0,  $IC_{50}$ , and  $1\frac{1}{2}IC_{50}$ ;  $\mu$ M;  $IC_{50}$  values obtained from the proliferation studies with cells of the same line) on phosphorylated protein levels after 48 h of treatment. (B) The data shown are immunoblots from three independent experiments. Rab-11 was used as loading control to confirm the loading uniformity. To obtain the bar graphs, the actual protein optical density values were normalized against those for loading control, and the resulting values are presented as a percentage of the corresponding ratios for untreated controls (mean  $\pm$  SD of relative quantitative density ratios). Statistical significance was assessed using one-way ANOVA and Dunn's multiple comparison tests; p < .01 (\*\*) and p < .001 (\*\*\*), as indicated, were each considered significant.

the in silico target fishing and docking experiments, it was conjectured that these two compounds exert their antiproliferative activities by interfering with CDK8, CLK4,

nuclear receptor ROR, tyrosine protein-kinase Fyn/LCK, ROCK1/2, and PARP, among other potential targets, all of which are dysregulated in skin cancers. The treatments of

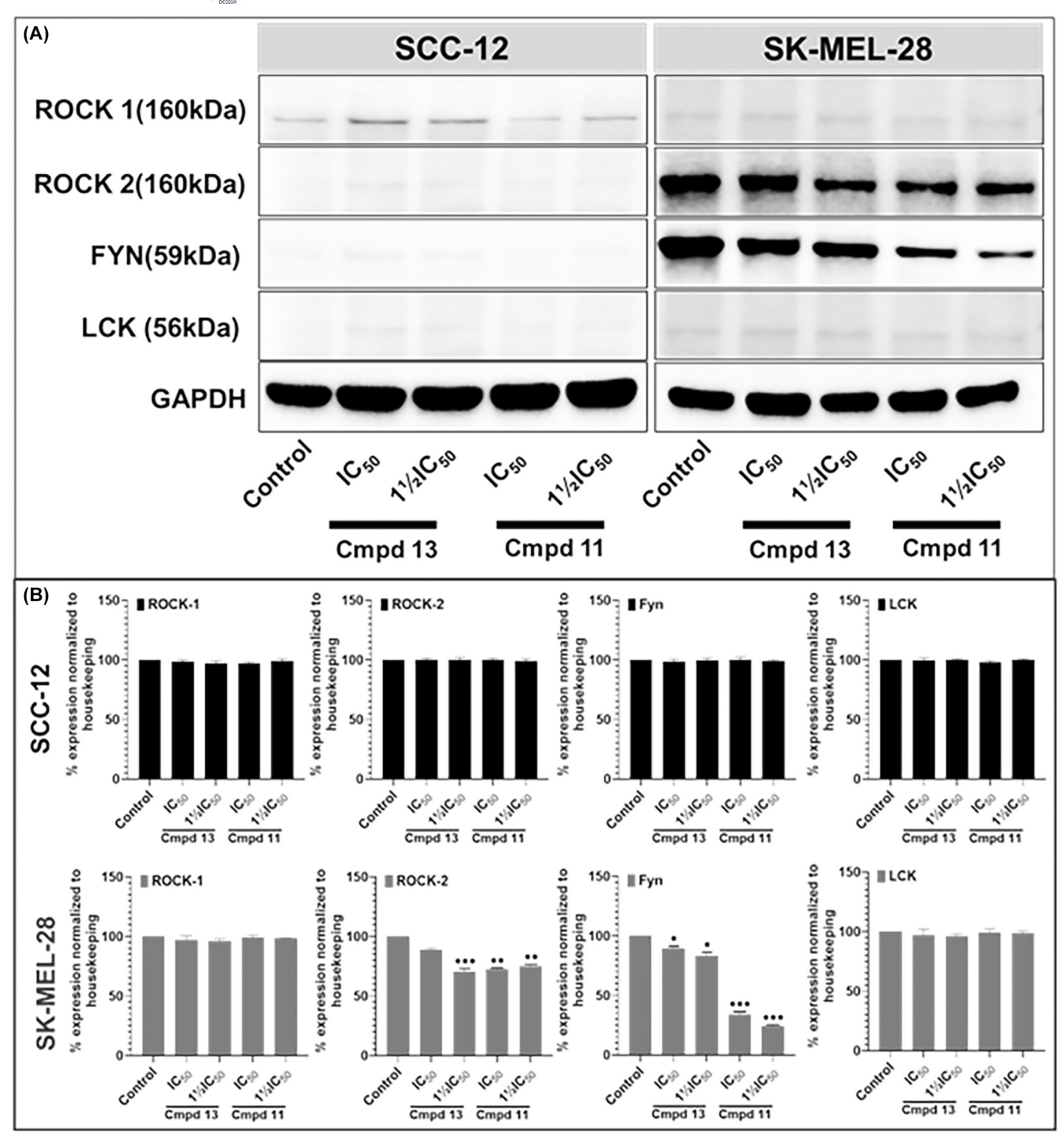


FIGURE 10 Validation of ROCK-1, ROCK-2, Fyn, and LCK as potential targets for compounds 11 and 13 in cutaneous melanoma (SK-MEL-28) and nonmelanoma (SCC-12) skin cancer cells, as suggested by significant interactions and binding affinity observed during the in silico studies. (A) Western blots show a dose-dependent effect (0, IC $_{50}$ , and  $1\frac{1}{2}$ IC $_{50}$ ;  $\mu$ M; IC $_{50}$  values obtained from the proliferation studies with cells of the same line) on protein levels after 48 h of treatment. (B) The data shown is immunoblots from three independent experiments. GAPDH was used as a loading control to confirm the loading uniformity. The actual protein optical density values were normalized against those for loading control to obtain the bar graphs. The resulting values are presented as a percentage of the corresponding ratios for untreated controls (mean  $\pm$  SD of relative quantitative density ratios). Statistical significance was assessed using one-way ANOVA and Dunn's multiple comparison tests; p < .01 (\*\*) and p < .001 (\*\*\*), as indicated, were each considered significant.

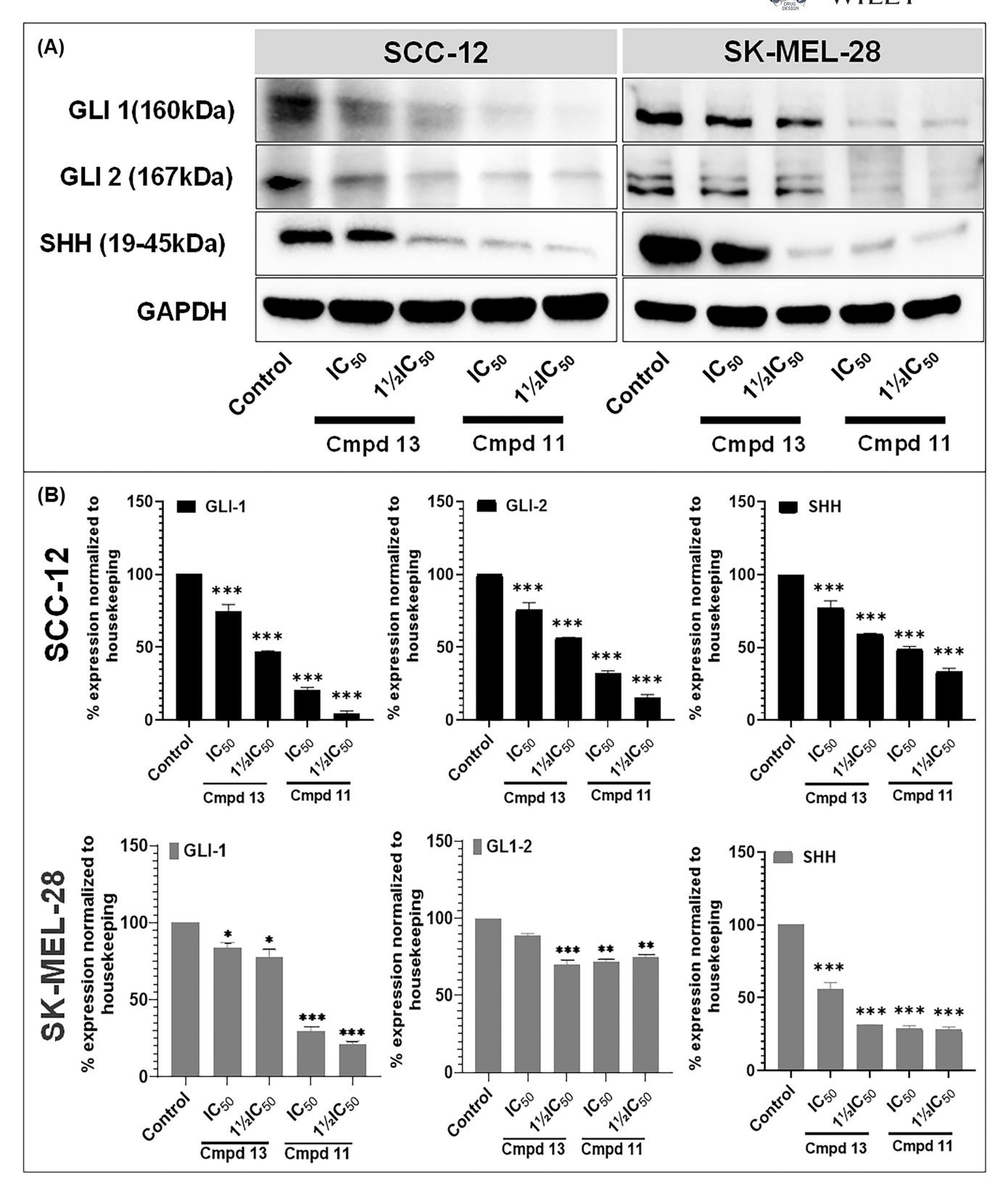


FIGURE 11 Compounds 11 and 13 can modulate the hedgehog signaling targets GLI 1, GLI 2 and SHH in cutaneous melanoma (SK-MEL-28) and nonmelanoma (SCC-12) skin cancer cells. (A) Western blots show a dose-dependent effect (0, IC $_{50}$  and  $1\frac{1}{2}$ IC $_{50}$ ;  $\mu$ M; IC $_{50}$  values obtained from the proliferation studies with cells of the same line) on protein levels after 48 h of treatment. (B) The data shown are immunoblots from three independent experiments. GAPDH was used as a loading control to confirm the loading uniformity. To obtain the bar graphs, the actual protein optical density values were normalized against those for loading control. The resulting values are presented as a percentage of the corresponding ratios for untreated controls (mean  $\pm$ SD of relative quantitative density ratios). Statistical significance was assessed using one-way ANOVA and Dunn's multiple comparison tests; p < .01 (\*\*) and p < .001 (\*\*\*), as indicated, were each considered significant.

SCC-12 and SK-MEL-28 with escalating concentrations of **11** or **13** (0, IC<sub>50</sub>, and 1½IC<sub>50</sub>; values for IC<sub>50</sub> from the cell proliferation experiments) for 48h resulted in a significant reduction in the levels of ROCK1, ROCK2, FYN, LCK, (Figure 10), GLI 1, GLI 2, and SHH (Figure 11) in a dose-dependent manner, as compared to the controls. Together, these data suggest that the downregulation of the Hedgehog (HH) pathway, rock and its upstream PI3K/AKT cascade might be an important target for these hit molecules. Although this might as well be only one among many other potential targets, it provides a solid framework for a rational design of analogs needed to optimize the anticancer properties of this family of compounds.

# 4 | CONCLUSIONS

In an effort to repurpose molecules previously prepared in our lab as part of a study of the biochemistry of Plasmodium falciparum, the parasite responsible for malaria, a combination of in vitro assays, in silico target fishing and docking studies were used to identify and map out the antiproliferative activity of hit compounds from this small library. A number of these compounds were identified to possess an optimizable antiproliferative activity when evaluated in vitro against melanoma (A375 and SK-MEL-28) and nonmelanoma (A431 and SCC-12) skin cancer cell lines. In silico target fishing studies using the SwissTargetPrediction tool indicated that many of these compounds have favorable physicochemical properties. In combination with docking predictions, these data suggested that CDK8, CLK4, nuclear receptor ROR, tyrosine protein-kinase Fyn/LCK, ROCK1/2, and PARP might be prospective molecular targets for the two most active compounds (11 and 13). Scratch wound-healing and colony formation functional/phenotypic assays indicated that compounds 11 and 13 exert their activity by interfering with the apoptotic pathways. At the same time, further western blot analyses suggested that ROCK/Fyn and the Hedgehog (Hh) pathway might be involved in the mechanisms of the action of the two lead compounds. The Hedgehog pathway is a central regulator of many fundamental processes in vertebrate embryonic development, including stem cell maintenance, cell differentiation, tissue polarity, and cell proliferation. While its role in organogenesis is decisive for proper embryonic development, mutation can rekindle its hyper-activation in many cancers (Girardi et al., 2019; Onishi et al., 2022). Cross-talk between the dysregulated HH and other crucial pathways such as the PI3K/Akt/mTOR, Rho GTPase (ROCK1/2) and Src family kinases (Fyn/

LCK) have been shown to amplify the invasiveness, metastatic, and chemo-resistance of tumors (Larsen & Moeller, 2020; Pecora et al., 2021). Extracellular matrix remodeling and cytoskeleton components (including microtubules, actin filaments, and intermediate filaments) are often affected by these signaling interactions and tend to downregulate or upregulate cell migration, anoikis/apoptosis modulators such as caspases, Bax, and PARP (Ma et al., 2022; Mengie Ayele et al., 2022). Small molecules that directly modulate HH and its related signaling pathways are potential chemotherapeutic agents, as their inhibition effects can result in a decrease in disease prognosis. While the data reported here is still preliminary, and the target mentioned above might be just one target among many others, this report illustrates how unsuspected biological activities of a class of compounds can be uncovered and quickly mapped out using a multifaceted approach. This study also provides a strong framework for a rationale design of new analogs for a comprehensive structure-activity relationship study, potentially leading to optimizing the anticancer activity of these two family.

### **ACKNOWLEDGMENTS**

None.

#### **FUNDING INFORMATION**

The authors acknowledge the financial support of NSF CHE-1954734 and from the Edward G. Schlieder Educational Foundation (awarded to JF). The following grants and funding partially supported this work: a Start-up fund from the University of Louisiana at Monroe (ULM) College of Pharmacy (COP), and a Faculty Research Seed grant #5CALHN-260615 awards from the ULMCOP; a Pilot and a full research project awards from a Louisiana Biomedical Research Network (LBRN)-IDeA Networks of Biomedical Research Excellence (INBRE) award from the National Institute of General Medical Sciences of the National Institutes of Health (NIGMS/NIH) grant number P2O GM103424-18, an LBRN-INBRE-COBRE Administrative Supplement Award from NIGMS/NIH grant 3P20GM103424-18S1, and a Louisiana Board of Regents Support Fund grant LEQSF (2021-24)-RD-A-22 (awarded to JCC). The content is solely the authors' responsibility and does not necessarily represent the official views of the funding agencies.

# CONFLICT OF INTEREST STATEMENT

The authors declare no known competing financial interests or personal relationships that could have appeared to influence the work reported in this paper.

### DATA AVAILABILITY STATEMENT

The following supporting information can be downloaded at Appendix S1, Table 1: Binding affinity of the hit compounds toward enzymes and phosphodiesterases as compared to natural or commercial ligands (in silico experiments); Table 2: Binding affinity of the hit compounds toward kinases, proteases, oxidoreductases, and erasers as compared to natural or commercial ligands; synthesis and characterization of compounds, <sup>1</sup>H-NMR, <sup>13</sup>C-NMR, and HRESIMS spectra of each of the compounds described in this report; raw western blot images.

## ORCID

Jean Fotie https://orcid.org/0000-0002-3404-4533 Jean Christopher Chamcheu https://orcid. org/0000-0002-3927-5664

## REFERENCES

- Acevedo-Diaz, A., Morales-Caban, B. M., Zayas-Santiago, A., Martinez-Montemayor, M. M., & Suarez-Arroyo, I. J. (2022). SCAMP3 regulates EGFR and promotes proliferation and migration of triple-negative breast cancer cells through the modulation of AKT, ERK, and STAT3 signaling pathways. *Cancers*, *14*(11), 2807. https://doi.org/10.3390/cancers14112807
- Adinolfi, B., Romanini, A., Vanni, A., Martinotti, E., Chicca, A., Fogli, S., & Nieri, P. (2013). Anticancer activity of anandamide in human cutaneous melanoma cells. *European Journal of Pharmacology*, 718(1–3), 154–159. https://doi.org/10.1016/j.ej-phar.2013.08.039
- Agbai, O. N., Buster, K., Sanchez, M., Hernandez, C., Kundu, R. V., Chiu, M., Roberts, W. E., Draelos, Z. D., Bhushan, R., Taylor, S. C., & Lim, H. W. (2014). Skin cancer and photoprotection in people of color: A review and recommendations for physicians and the public. *Journal of the American Academy of Dermatology*, 70(4), 748–762. https://doi.org/10.1016/j.jaad. 2013.11.038
- Almeida, E. R., & Dos Santos, H. F. (2023). Nanoconfinement effect on the hydrolysis of cisplatin. *Chemical Physics Letters*, *811*, 140247. https://doi.org/10.1016/j.cplett.2022.140247
- An, S., Kim, K., Moon, S., Ko, K.-P., Kim, I., Lee, J. E., & Park, S. K. (2021). Indoor tanning and the risk of overall and early-onset melanoma and non-melanoma skin cancer: Systematic review and meta-analysis. *Cancers*, 13(23), 5940. https://doi.org/10.3390/cancers13235940
- Aranha, E. S. P., Portilho, A. J. D. S., Bentes de Sousa, L., da Silva, E. L., Mesquita, F. P., Rocha, W. C., da Araújo Silva, F. M., Lima, E. S., Alves, A. P. N. N., Koolen, H. H. F., Montenegro, R. C., & Carvalho de Vasconcellos, M. (2021). 22β-hydroxytingenone induces apoptosis and suppresses invasiveness of melanoma cells by inhibiting MMP-9 activity and MAPK signaling. *Journal of Ethnopharmacology*, 267, 113605. https://doi.org/10.1016/j.jep. 2020.113605
- Armstrong, M. S., Finn, P. W., Morris, G. M., & Richards, W. G. (2011). Improving the accuracy of ultrafast ligand-based screening: Incorporating lipophilicity into ElectroShape as an extra dimension. *Journal of Computer-Aided Molecular*

- Design, 25(8), 785–790. https://doi.org/10.1007/s1082 2-011-9463-8
- Armstrong, M. S., Morris, G. M., Finn, P. W., Sharma, R., Moretti, L., Cooper, R. I., & Richards, W. G. (2010). ElectroShape: Fast molecular similarity calculations incorporating shape, chirality and electrostatics. *Journal of Computer-Aided Molecular Design*, 24(9), 789–801. https://doi.org/10.1007/s10822-010-9374-0
- Arnold, M., de Vries, E., Whiteman, D. C., Jemal, A., Bray, F., Parkin, D. M., & Soerjomataram, I. (2018). Global burden of cutaneous melanoma attributable to ultraviolet radiation in 2012. *International Journal of Cancer*, 143(6), 1305–1314. https://doi.org/10.1002/ijc.31527
- Ascierto, P. A., & Garbe, C. (2020). Updates and new perspectives in nonmelanoma skin cancer therapy: Highlights from 'immunotherapy bridge'. *Immunotherapy*, 12(3), 167–174. https://doi.org/10.2217/imt-2020-0042
- Audrito, V., Messana, V. G., Moiso, E., Vitale, N., Arruga, F., Brandimarte, L., Gaudino, F., Pellegrino, E., Vaisitti, T., Riganti, C., Piva, R., & Deaglio, S. (2020). NAMPT over-expression recapitulates the BRAF inhibitor resistant phenotype plasticity in melanoma. *Cancers*, 12(12), 3855. https://doi.org/10.3390/cancers12123855
- Baell, J. B., & Holloway, G. A. (2010). New substructure filters for removal of pan-assay interference compounds (PAINS) from screening libraries and for their exclusion in bioassays. *Journal* of Medicinal Chemistry, 53(7), 2719–2740. https://doi.org/10. 1021/jm901137j
- Baell, J. B., & Nissink, J. W. M. (2018). Seven year itch: Pan-assay interference compounds (PAINS) in 2017 utility and limitations. ACS Chemical Biology, 13(1), 36–44. https://doi.org/10.1021/acschembio.7b00903
- Berkessa, S. C., Clarke, Z. J. F., Fotie, J., Bohle, D. S., & Grimm, C. C. (2016). Silver(I)-mediated regioselective oxidative cross-coupling of phenol and aniline derivatives resulting in 2'-aminobiphenyl-2-ols. *Tetrahedron Letters*, 57(14), 1613–1618. https://doi.org/10.1016/j.tetlet.2016.02.111
- Beroukhim, K., Pourang, A., & Eisen, D. B. (2020). Risk of second primary cutaneous and noncutaneous melanoma after cutaneous melanoma diagnosis: A population-based study. *Journal of the American Academy of Dermatology*, 82(3), 683–689. https://doi.org/10.1016/j.jaad.2019.10.024
- Boice, A., & Bouchier-Hayes, L. (2020). Targeting apoptotic caspases in cancer. *Biochimica et Biophysica Acta, Molecular Cell Research*, 1867(6), 118688. https://doi.org/10.1016/j.bbamcr. 2020.118688
- Brandl, L., Hartmann, D., Kirchner, T., & Menssen, A. (2019).
  Expression of n-MYC, NAMPT and SIRT1 in basal cell carcinomas and their cells of origin. *Acta Dermato-Venereologica*, 99(1), 63–71. https://doi.org/10.2340/00015555-3031
- Brozyna, A. A., Brozyna, A. A., Jozwicki, W., Jozwicki, W., Jetten, A. M., Slominski, A. T., & Slominski, A. T. (2019). On the relationship between VDR, ROR $\alpha$  and ROR $\gamma$  receptors expression and HIF1- $\alpha$  levels in human melanomas. *Experimental Dermatology*, 28(9), 1036–1043.
- Brozyna, A. A., Jozwicki, W., Brozyna, A. A., Jozwicki, W., Skobowiat, C., Jetten, A., & Slominski, A. T. (2016). ROR $\alpha$  and ROR $\gamma$  expression inversely correlates with human melanoma progression. *Oncotarget*, 7(39), 63261–63282.
- Brummer, T., Martin, P., Herzog, S., Misawa, Y., Daly, R. J., & Reth, M. (2006). Functional analysis of the regulatory requirements

- of B-Raf and the B-RafV600E oncoprotein. *Oncogene*, 25(47), 6262–6276. https://doi.org/10.1038/sj.onc.1209640
- Burley, S. K., Berman, H. M., Christie, C., Duarte, J. M., Feng, Z., Westbrook, J., Young, J., & Zardecki, C. (2018). RCSB Protein Data Bank: Sustaining a living digital data resource that enables breakthroughs in scientific research and biomedical education. *Protein Science*, *27*(1), 316–330. https://doi.org/10.1002/pro.3331
- Carvajal, R. D., Butler, M. O., Shoushtari, A. N., Hassel, J. C., Ikeguchi, A., Hernandez-Aya, L., Carvajal, R. D., Nathan, P., Hamid, O., Piulats, J. M., Rioth, M., Johnson, D. B., Luke, J. J., Espinosa, E., Leyvraz, S., Collins, L., Goodall, H. M., Ranade, K., Holland, C., ... Sato, T. (2022). Clinical and molecular response to tebentafusp in previously treated patients with metastatic uveal melanoma: A phase 2 trial. *Nature Medicine*, 28(11), 2364–2373. https://doi.org/10.1038/s41591-022-02015-7
- Casanova, M. L., Blazquez, C., Martinez-Palacio, J., Villanueva, C., Fernandez-Acenero, M. J., Huffman, J. W., Jorcano, J. L., & Guzman, M. (2003). Inhibition of skin tumor growth and angiogenesis in vivo by activation of cannabinoid receptors. *Journal of Clinical Investigation*, 111(1), 43–50. https://doi.org/10.1172/JCI16116
- Chamcheu, J. C., Esnault, S., Adhami, V. M., Noll, A. L., Banang-Mbeumi, S., Roy, T., Singh, S. S., Huang, S., Kousoulas, K. G., & Mukhtar, H. (2019). Fisetin, a 3,7,3',4'-tetrahydroxyflavone inhibits the PI3K/Akt/mTOR and MAPK pathways and ameliorates psoriasis pathology in 2D and 3D organotypic human inflammatory skin models. *Cells*, 8(9), 1089. https://doi.org/10.3390/cells8091089
- Chamcheu, J. C., Roy, T., Uddin, M. B., Banang-Mbeumi, S., Chamcheu, R.-C. N., Walker, A. L., Liu, Y.-Y., & Huang, S. (2019). Role and therapeutic targeting of the PI3K/Akt/mTOR signaling pathway in skin cancer: A review of current status and future trends on natural and synthetic agents therapy. *Cells*, 8(8), 803. https://doi.org/10.3390/cells8080803
- Chang, F., Zhang, Y., Mi, J., Zhou, Q., Bai, F., Xu, X., Fisher, D. E., Sun, Q., & Wu, X. (2018). ROCK inhibitor enhances the growth and migration of BRAF-mutant skin melanoma cells. *Cancer Science*, 109(11), 3428–3437. https://doi.org/10.1111/cas.13786
- Chen, C., Li, Y., Hou, S., Bourbon, P. M., Qin, L., Zhao, K., Ye, T., Zhao, D., Zeng, H., & Zeng, H. (2020). Orphan nuclear receptor TR3/Nur77 biologics inhibit tumor growth by targeting angiogenesis and tumor cells. *Microvascular Research*, 128, 103934. https://doi.org/10.1016/j.mvr.2019.103934
- Colantonio, S., Bracken, M. B., & Beecker, J. (2014). The association of indoor tanning and melanoma in adults: Systematic review and meta-analysis. *Journal of the American Academy of Dermatology*, 70(5), 847–857.e1–18. https://doi.org/10.1016/j.jaad.2013.11.050
- Dabrowska, C., Li, M., & Fan, Y. (2016). Apoptotic caspases in promoting cancer: Implications from their roles in development and tissue homeostasis. *Advances in Experimental Medicine and Biology*, *930*, 89–112. https://doi.org/10.1007/978-3-319-39406-0\_4
- Daina, A., Michielin, O., & Zoete, V. (2014). iLOGP: A simple, robust, and efficient description of n-octanol/water partition coefficient for drug design using the GB/SA approach. *Journal of Chemical Information and Modeling*, 54(12), 3284–3301. https://doi.org/10.1021/ci500467k

- Daina, A., Michielin, O., & Zoete, V. (2019). SwissTargetPrediction: Updated data and new features for efficient prediction of protein targets of small molecules. *Nucleic Acids Research*, *47*(W1), W357–W364. https://doi.org/10.1093/nar/gkz382
- Daina, A., Michielin, O., Zoete, V., Michielin, O., & Michielin, O. (2017). SwissADME: A free web tool to evaluate pharmacokinetics, drug-likeness and medicinal chemistry friendliness of small molecules. *Scientific Reports*, 7, 42717.
- Dennis, L. K., Vanbeek, M. J., Beane Freeman, L. E., Smith, B. J., Dawson, D. V., & Coughlin, J. A. (2008). Sunburns and risk of cutaneous melanoma: Does age matter? A comprehensive meta-analysis. *Annals of Epidemiology*, 18(8), 614–627. https://doi.org/10.1016/j.annepidem.2008.04.006
- DePalo, D. K., Tarhini, A., & Zager, J. S. (2022). The treatment of advanced melanoma: A review of systemic and local therapies in combination with immune checkpoint inhibitors in phase 1 and 2 clinical trials. *Expert Opinion on Investigational Drugs*, 31(1), 95–104. https://doi.org/10.1080/13543784.2022.2027366
- Dickson, M. A., Hahn, W. C., Ino, Y., Ronfard, V., Wu, J. Y., Weinberg, R. A., Louis, D. N., Li, F. P., & Rheinwald, J. G. (2000). Human keratinocytes that express hTERT and also bypass a p16INK4a-enforced mechanism that limits life span become immortal yet retain normal growth and differentiation characteristics. *Molecular and Cellular Biology*, 20(4), 1436–1447. https://doi.org/10.1128/mcb.20.4.1436-1447.2000
- Donati, M., Michal, M., Donati, M., Martinek, P., Kastnerova, L., Michal, M., & Michal, M. (2020). RAF1 gene fusions as a possible driver mechanism in rare BAP1-inactivated melanocytic tumors: A report of 2 cases. *American Journal of Dermatopathology*, 42(12), 961–966.
- Dong, X., Akuetteh, P. D. P., Song, J., Ni, C., Jin, C., Li, H., Jiang, W., Si, Y., Zhang, X., Zhang, Q., & Huang, G. (2021). Major vault protein (MVP) associated with BRAFV600E mutation is an immune microenvironment-related biomarker promoting the progression of papillary thyroid cancer via MAPK/ERK and PI3K/AKT pathways. *Frontiers in Cell and Developmental Biology*, 9, 688370. https://doi.org/10.3389/fcell.2021.688370
- Egan, W. J., Merz, K. M., Jr., & Baldwin, J. J. (2000). Prediction of drug absorption using multivariate statistics. *Journal of Medicinal Chemistry*, *43*(21), 3867–3877. https://doi.org/10. 1021/jm000292e
- Enane, F. O., Saunthararajah, Y., & Korc, M. (2018). Differentiation therapy and the mechanisms that terminate cancer cell proliferation without harming normal cells. *Cell Death & Disease*, 9(9), 1–15. https://doi.org/10.1038/s41419-018-0919-9
- Fathi, A. T., Le, L., Hasserjian, R. P., Sadrzadeh, H., Levis, M., & Chen, Y.-B. (2013). FLT3 inhibitor-induced neutrophilic dermatosis. *Blood*, *122*(2), 239–242. https://doi.org/10.1182/blood-2013-01-478172
- Fotie, J. (2012). Key natural products in malaria chemotherapy: From quinine to artemisinin and beyond. In G. Brahmachari (Ed.), *Bioactive natural products: Opportunities and challenges in medicinal chemistry* (pp. 223–271). World Scientific Publishing.
- Fotie, J. (2018). Inosine 5'-monophosphate dehydrogenase (IMPDH) as a potential target for the development of a new generation of antiprotozoan agents. *Mini-Reviews in Medicinal Chemistry*, 18(8), 656–671. https://doi.org/10.2174/138955751666616 0620065558

- Fotie, J. (2019). Marine natural products as strategic prototypes in the development of a new generation of antimalarial agents. In G. Brahmachari (Ed.), *Chapter 2: Discovery and development of therapeutics from natural products against neglected tropical diseases* (pp. 8–47). Elsevier.
- Fotie, J., Ayer, S. K., Poudel, B. S., & Reid, C. S. (2013). Iodine-catalyzed cycloalkenylation of dihydroquinolines and arylamines through a reaction with cyclic ketones under neat conditions. *Tetrahedron Letters*, 54(51), 7069–7073. https://doi.org/10.1016/j.tetlet.2013.10.081
- Fotie, J., Kemami Wangun, H. V., Fronczek, F. R., Massawe, N., Bhattarai, B. T., Rhodus, J. L., Ingleton, T., & Bohle, D. S. (2012). Unexpected 6,6-pentamethylene-5,6,7,8,9,10-hexahydrophena nthridines and 2,3,4,5-tetrahydro-4,4-tetramethylene-1*H*-cyclo penta[*c*]quinolones from the Skraup Doebner Von Miller quinolone synthesis, and their implications for the mechanism of that reaction. *The Journal of Organic Chemistry*, 77(6), 2784–2790. https://doi.org/10.1021/jo202681r
- Fotie, J., Olvera, A., Ayer, S. K., Djieutedjeu, H., & Poudeu, P. F. P. (2015). Synthesis and crystal structures of methyl 3,4,5-trimethoxybenzoate and 1,2-dihydro-2,2,4-trimethylquin oline derivatives. *Journal of Chemical Crystallography*, 45(1), 1–8. https://doi.org/10.1007/s10870-014-0556-9
- Fotie, J., Rhodus, J. L., Taha, H. A., & Reid, C. S. (2012). C-N coupling of 1,2-dihydro-2,2,4-trimethylquinoline derivatives via a silver(I)-catalyzed direct functionalization of a C-H bond. Heteroatom Chemistry, 23(6), 598–604. https://doi.org/10.1002/hc.21055
- Gfeller, D., Grosdidier, A., Wirth, M., Daina, A., Michielin, O., & Zoete, V. (2014). SwissTargetPrediction: A web server for target prediction of bioactive small molecules. *Nucleic Acids Research*, 42(W1), W32–W38. https://doi.org/10.1093/nar/gku293
- Ghose, A. K., Viswanadhan, V. N., & Wendoloski, J. J. (1999). A knowledge-based approach in designing combinatorial or medicinal chemistry libraries for drug discovery. 1. A qualitative and quantitative characterization of known drug databases. *Journal of Combinatorial Chemistry*, 1(1), 55–68. https://doi. org/10.1021/CC9800071
- Girardi, D., Barrichello, A., Fernandes, G., & Pereira, A. (2019). Targeting the hedgehog pathway in cancer: Current evidence and future perspectives. *Cells*, 8(2), 153. https://doi.org/10.3390/cells8020153
- Guy, G. P., Jr., Machlin, S. R., Ekwueme, D. U., & Yabroff, K. R. (2015). Prevalence and costs of skin cancer treatment in the US, 2002–2006 and 2007–2011. *American Journal of Preventive Medicine*, 48, 183–187. https://doi.org/10.1016/j.amepre.2014. 08.036
- Guy, G. P., Jr., Thomas, C. C., Thompson, T., Watson, M., Massetti, G. M., & Richardson, L. C. (2015). Vital signs: Melanoma incidence and mortality trends and projections - United States, 1982–2030. The Morbidity and Mortality Weekly Report, 64(21), 591–596.
- Han, X., Han, Y., Zheng, Y., Sun, Q., Ma, T., Dai, L., Zhang, J., & Xu, L. (2018). Use of phosphodiesterase type 5 inhibitors and risk of melanoma: A meta-analysis of observational studies. OncoTargets and Therapy, 11, 1–10. https://doi.org/10.2147/ott.s142637
- Harris, R., Olson, A. J., & Goodsell, D. S. (2008). Automated prediction of ligand-binding sites in proteins. *Proteins: Structure*,

- Function, and Bioinformatics, 70(4), 1506–1517. https://doi.org/10.1002/prot.21645
- Hwang, S.-Y., Chae, J.-I., Kwak, A.-W., Lee, M.-H., & Shim, J.-H. (2020). Alternative options for skin cancer therapy via regulation of AKT and related signaling pathways. *International Journal of Molecular Sciences*, 21(18), 6869. https://doi.org/10.3390/ijms21186869
- Islami, F., Sauer, A. G., Miller, K. D., Fedewa, S. A., Minihan, A. K., Geller, A. C., Lichtenfeld, J. L., & Jemal, A. (2020). Cutaneous melanomas attributable to ultraviolet radiation exposure by state. *International Journal of Cancer*, *147*(5), 1385–1390. https://doi.org/10.1002/ijc.32921
- Jeric, I., Maurer, G., Cavallo, A. L., Raguz, J., Desideri, E., Tarkowski, B., Matthias Parrini, M., Fischer, I., Zatloukal, K., & Baccarini, M. (2016). A cell-autonomous tumour suppressor role of RAF1 in hepatocarcinogenesis. *Nature Communications*, 7, 13781. https://doi.org/10.1038/ncomms13781
- Kaczorowski, M., Biecek, P., Donizy, P., Pieniazek, M., Matkowski, R., & Halon, A. (2020). ROCK1 and ROCK2 are down-regulated in aggressive and advanced skin melanomas - a clinicopathological perspective. *Anticancer Research*, 40(4), 1931–1942. https://doi.org/10.21873/anticanres.14148
- Kakish, H. H., Ahmed, F. A., Elshami, M., Loftus, A. W., Hoehn, R. S., Ammori, J. B., Ocuin, L. M., Winter, J. M., Bordeaux, J. S., Mangla, A., & Rothermel, L. D. (2022). Trends in melanoma phase 3 clinical trials since 2010: Is there hope for advanced melanoma therapies beyond approved treatment mechanisms? *Cancers*, 14(21), 5184. https://doi.org/10.3390/cancers142 15184
- Katikaneni, A., Jelcic, M., Gerlach, G. F., Ma, Y., Overholtzer, M., & Niethammer, P. (2020). Lipid peroxidation regulates long-range wound detection through 5-lipoxygenase in zebrafish. *Nature Cell Biology*, 22(9), 1049–1055. https://doi.org/10.1038/s41556-020-0564-2
- Khasabova, I. A., Khasabov, S. G., Harding-Rose, C., Coicou, L. G., Seybold, B. A., Lindberg, A. E., Steevens, C. D., Simone, D. A., & Seybold, V. S. (2008). A decrease in anandamide signaling contributes to the maintenance of cutaneous mechanical hyperalgesia in a model of bone cancer pain. *Journal of Neuroscience*, 28(44), 11141–11152. https://doi.org/10.1523/JNEUROSCI. 2847-08.2008
- Lagorce, D., Sperandio, O., Baell, J. B., Miteva, M. A., & Villoutreix, B. O. (2015). FAF-Drugs3: A web server for compound property calculation and chemical library design. *Nucleic Acids Research*, *43*(W1), W200–W207. https://doi.org/10.1093/nar/gkv353
- Larsen, L. J., & Moeller, L. B. (2020). Crosstalk of hedgehog and mTORC1 pathways. *Cells*, 9(10), 2316. https://doi.org/10.3390/cells9102316
- Lee, K. (2019). JAAD game changers: The association of indoor tanning and melanoma in adults: Systematic review and meta-analysis. *Journal of the American Academy of Dermatology*, 88, 749. https://doi.org/10.1016/j.jaad.2019.11.050
- Lipinski, C. A., Lombardo, F., Dominy, B. W., & Feeney, P. J. (2001). Experimental and computational approaches to estimate solubility and permeability in drug discovery and development settings. *Advanced Drug Delivery Reviews*, 46(1–3), 3–26. https://doi.org/10.1016/S0169-409X(00)00129-0
- Lopez, A., Reyna, D. E., Gitego, N., Kopp, F., Zhou, H., Miranda-Roman, M. A., Nordstrøm, L. U., Narayanagari, S. R., Chi, P., Vilar, E., Tsirigos, A., & Gavathiotis, E. (2022). Co-targeting

- of BAX and BCL-XL proteins broadly overcomes resistance to apoptosis in cancer. *Nature Communications*, *13*(1), 1199. https://doi.org/10.1038/s41467-022-28741-7
- Luo, Y., Zhang, D., Hou, L., & Lin, N. (2022). Vernodalin suppresses tumor proliferation and increases apoptosis of gastric cancer cells through attenuation of FAK/PI3K/AKT/mTOR and MAPKs signaling pathways. *Current Pharmaceutical Biotechnology*, 24(5), 708–717. https://doi.org/10.2174/13892 01023666220728150544
- Ma, R.-J., Ma, C., Hu, K., Zhao, M.-M., Zhang, N., & Sun, Z.-G. (2022). Molecular mechanism, regulation, and therapeutic targeting of the STAT3 signaling pathway in esophageal cancer (review). *International Journal of Oncology*, 61(3), 105. https://doi.org/10.3892/ijo.2022.5395
- Martens, M. C., Seebode, C., Lehmann, J., & Emmert, S. (2018). Photocarcinogenesis and skin cancer prevention strategies: An update. *Anticancer Research*, *38*(2), 1153–1158. https://doi.org/10.21873/anticanres.12334
- Mengie Ayele, T., Tilahun Muche, Z., Behaile Teklemariam, A., Bogale Kassie, A., & Chekol Abebe, E. (2022). Role of JAK2/STAT3 signaling pathway in the tumorigenesis, chemotherapy resistance, and treatment of solid tumors: A systemic review. *Journal of Inflammation Research*, *15*, 1349–1364. https://doi.org/10.2147/jir.s353489
- Miller, K. D., Nogueira, L., Devasia, T., Mariotto, A. B., Yabroff, K. R., Jemal, A., Kramer, J., & Siegel, R. L. (2022). Cancer treatment and survivorship statistics, 2022. *Cancer Journal for Clinicians*, 72(5), 409–436. https://doi.org/10.3322/caac. 21731
- Muegge, I., Heald, S. L., & Brittelli, D. (2001). Simple selection criteria for drug-like chemical matter. *Journal of Medicinal Chemistry*, 44(12), 1841–1846. https://doi.org/10.1021/jm015507e
- Mulvaney, P. M., & Schmults, C. D. (2020). Molecular prediction of metastasis in cutaneous squamous cell carcinoma. *Current Opinion in Oncology*, 32(2), 129–136. https://doi.org/10.1097/ CCO.0000000000000000000009
- Murahari, M. S., & Yergeri, M. C. (2014). Current overview on the usage of poly(ADP-ribose)polymerase (PARP) inhibitors in treating cancer. *Clinical Cancer Drugs*, 1(2), 127–148. https://doi.org/10.2174/2212697X01666140128002849
- Nair, P. P. S., Chandrashekarappa, K. K. H., Masagalli, J. N., Nagaraja, P., & Mahadevan, K. M. (2015). Toxicity and molecular docking studies of tetrahydroquinolines against microbial, cancer, retinoic acid receptor, inflammatory, cholesterol ester transferases and parasitic protein receptors. *International Journal of Pharmacy and Pharmaceutical Sciences*, 7(2), 448–459.
- Onishi, H., Nakamura, K., Yanai, K., Nagai, S., Nakayama, K., Oyama, Y., Fujimura, A., Ozono, K., & Yamasaki, A. (2022). Cancer therapy that targets the Hedgehog signaling pathway considering the cancer microenvironment (review). *Oncology Reports*, 47(5), 93. https://doi.org/10.3892/or.2022.8304
- Ozoran, E., Trabulus, F. D. C., Erhan, D., Batar, B., & Guven, M. (2022). Association of XRCC3, XRCC4, BAX, and BCL-2 polymorphisms with the risk of breast cancer. *International Journal of Breast Cancer*, 2022, 5817841. https://doi.org/10.1155/2022/5817841
- Paulson, K. G., Gupta, D., Kim, T. S., Veatch, J. R., Byrd, D. R., Bhatia, S., Wojcik, K., Chapuis, A. G., Thompson, J. A., Madeleine, M. M., & Gardner, J. M. (2020). Age-specific incidence of melanoma in the United States. *JAMA Dermatology*, 156(1), 57–64. https://doi.org/10.1001/jamadermatol.2019.3353

- Pavel, T. I., Chircov, C., Grumezescu, A. M., & Radulescu, M. (2020).
  Regenerative wound dressings for skin cancer. *Cancers*, 12(10), 2954. https://doi.org/10.3390/cancers12102954
- Pecora, A., Laprise, J., Dahmene, M., & Laurin, M. (2021). Skin cancers and the contribution of rho GTPase signaling networks to their progression. *Cancers*, *13*(17), 4362. https://doi.org/10.3390/cancers13174362
- Pisani, C., Ramella, M., Boldorini, R., Loi, G., Billia, M., Boccafoschi, F., Volpe, A., & Krengli, M. (2020). Apoptotic and predictive factors by Bax, caspases 3/9, Bcl-2, p53 and Ki-67 in prostate cancer after 12 Gy single-dose. *Scientific Reports*, *10*(1), 7050. https://doi.org/10.1038/s41598-020-64062-9
- Pisano, M., Palmieri, G., Rozzo, C., Dettori, M. A., Fabbri, D., & Delogu, G. (2021). Anticancer activity of two novel hydroxylated biphenyl compounds toward malignant melanoma cells. *International Journal of Molecular Sciences*, 22(11), 5636. https://doi.org/10.3390/ijms22115636
- Rheinwald, J. G., & Beckett, M. A. (1981). Tumorigenic keratinocyte lines requiring anchorage and fibroblast support cultured from human squamous cell carcinomas. *Cancer Research*, *41*(5), 1657–1663.
- Rigsby, R. E., & Parker, A. B. (2016). Using the PyMOL application to reinforce visual understanding of protein structure. Biochemistry and Molecular Biology Education, 44(5), 433–437. https://doi.org/10.1002/bmb.20966
- Robertson, B. F., Wokes, J. E. T., & Siddiqui, H. (2018). Management of incompletely excised skin tumors: Our experience. *Dermatologic Surgery*, 44(3), 365–369. https://doi.org/10.1097/ dss.0000000000001323
- Roy, T., Boateng, S. T., Banang-Mbeumi, S., Singh, P. K., Basnet,
  P., Chamcheu, R.-C. N., Ladu, F., Chauvin, I., Spiegelman,
  V. S., Hill, R. A., Kousoulas, K. G., Nagalo, B. M., Walker, A.
  L., Fotie, J., Murru, S., Sechi, M., & Chamcheu, J. C. (2021a).
  Identification of new fisetin analogs as kinase inhibitors: Data
  on synthesis and anti-skin cancer activities evaluation. *Data in Brief*, 35, 106858. https://doi.org/10.1016/j.dib.2021.106858
- Roy, T., Boateng, S. T., Banang-Mbeumi, S., Singh, P. K., Basnet, P., Chamcheu, R.-C. N., Ladu, F., Chauvin, I., Spiegelman, V. S., Hill, R. A., Kousoulas, K. G., Nagalo, B. M., Walker, A. L., Fotie, J., Murru, S., Sechi, M., & Chamcheu, J. C. (2021b). Synthesis, inverse docking-assisted identification and in vitro biological characterization of flavonol-based analogs of fisetin as c-kit, CDK2 and mTOR inhibitors against melanoma and non-melanoma skin cancers. *Bioorganic Chemistry*, 107, 104595. https://doi.org/10.1016/j.bioorg.2020.104595
- Saubern, S., Guha, R., & Baell, J. B. (2011). KNIME workflow to assess PAINS filters in SMARTS format. Comparison of RDKit and indigo cheminformatics libraries. *Molecular Informatics*, 30(10), 847–850. https://doi.org/10.1002/minf.201100076
- Shirakawa, T., Rojasawasthien, T., Inoue, A., Matsubara, T., Kawamoto, T., & Kokabu, S. (2021). Tumor necrosis factor alpha regulates myogenesis to inhibit differentiation and promote proliferation in satellite cells. *Biochemical and Biophysical Research Communications*, 580, 35–40. https://doi.org/10. 1016/j.bbrc.2021.09.067
- Siegel, R. L., Miller, K. D., Fuchs, H. E., & Jemal, A. (2022). Cancer statistics, 2022. *Cancer Journal for Clinicians*, 72(1), 7–33. https://doi.org/10.3322/caac.21708
- Spanbroek, R., Stark, H.-J., Janssen-Timmen, U., Kraft, S., Hildner, M., Andi, T., Bosch, F. X., Fusenig, N. E., Bieber, T., Rådmark,

- O., Samuelsson, B., & Habenicht, A. J. R. (1998). 5-Lipoxygenase expression in Langerhans cells of normal human epidermis. *Proceedings of the National Academy of Sciences of the United States of America*, 95(2), 663–668. https://doi.org/10.1073/pnas. 95.2.663
- Tang, C., Livingston, M. J., Safirstein, R., & Dong, Z. (2023). Cisplatin nephrotoxicity: New insights and therapeutic implications. *Nature Reviews Nephrology*, 19(1), 53–72. https://doi.org/10. 1038/s41581-022-00631-7
- Tang, H., Wu, W., Fu, S., Zhai, S., Song, Y., & Han, J. (2017). Phosphodiesterase type 5 inhibitors and risk of melanoma: A meta-analysis. *Journal of the American Academy of Dermatology*, 77(3), 480–488.e9. https://doi.org/10.1016/j.jaad. 2017.04.1129
- Tho, L. M., Libertini, S., Rampling, R., Sansom, O., & Gillespie, D. A. (2012). Chk1 is essential for chemical carcinogen-induced mouse skin tumorigenesis. *Oncogene*, 31(11), 1366–1375. https://doi.org/10.1038/onc.2011.326
- Trott, O., & Olson, A. J. (2010). AutoDock Vina: Improving the speed and accuracy of docking with a new scoring function, efficient optimization, and multithreading. *Journal of Computational Chemistry*, *31*(2), 455–461. https://doi.org/10.1002/jcc.21334
- Tu, T., Huang, J., Lin, M., Gao, Z., Wu, X., Zhang, W., Zhou, G., Wenbo Wang, W., & Liu, W. (2019). CUDC-907 reverses pathological phenotype of keloid fibroblasts in vitro and in vivo via dual inhibition of PI3K/Akt/mTOR signaling and HDAC2. *International Journal of Molecular Medicine*, 44(5), 1789–1800. https://doi.org/10.3892/ijmm.2019.4348
- Veber, D. F., Johnson, S. R., Cheng, H.-Y., Smith, B. R., Ward, K. W., & Kopple, K. D. (2002). Molecular properties that influence the oral bioavailability of drug candidates. *Journal of Medicinal Chemistry*, 45(12), 2615–2623. https://doi.org/10.1021/jm020 017n
- Vogeley, C., Esser, C., Tueting, T., Krutmann, J., & Haarmann-Stemmann, T. (2019). Role of the aryl hydrocarbon receptor in environmentally induced skin aging and skin carcinogenesis. *International Journal of Molecular Sciences*, *20*(23), 6005. https://doi.org/10.3390/ijms20236005
- Wang, M., Yue, Z., Paus, R., & Ramot, Y. (2014). SIRT2 as a new player in epigenetic programming of keratinocyte differentiation and a candidate tumor suppressor. *Experimental Dermatology*, 23(9), 636–638. https://doi.org/10.1111/exd.12434
- Wang, X., Zhou, Y., Wang, D., Wang, Y., Zhou, Z., Ma, X., Liu, X., & Dong, Y. (2023). Cisplatin-induced ototoxicity: From signaling network to therapeutic targets. *Biomedicine & Pharmacotherapy*, 157, 114045. https://doi.org/10.1016/j.bio-pha.2022.114045
- Wang, Z., Forsund, M. S., Trope, C. G., Nesland, J. M., Holm, R., & Slipicevic, A. (2018). Evaluation of CHK1 activation in vulvar

- squamous cell carcinoma and its potential as a therapeutic target in vitro. *Cancer Medicine*, 7(8), 3955–3964. https://doi.org/10.1002/cam4.1638
- Watson, R. W. G., Coffey, R., O'Neill, A., & Fitzpatrick, J. M. (1999).
  Caspase protease manipulation: A novel approach to apoptotic induction in prostate cancer. *Prostate Cancer and Prostatic Diseases*, 2(S3), S34. https://doi.org/10.1038/sj.pcan.4500359
- Wiechec, E., Magan, M., Matic, N., Ansell-Schultz, A., Kankainen, M., Monni, O., Johansson, A.-C., & Roberg, K. (2021). Cancerassociated fibroblasts modulate transcriptional signatures involved in proliferation, differentiation and metastasis in head and neck squamous cell carcinoma. *Cancers*, 13(13), 3361. https://doi.org/10.3390/cancers13133361
- Wohlman, I. M., Composto, G. M., Heck, D. E., Heindel, N. D., Lacey, C. J., Guillon, C. D., Casillas, R. P., Croutch, C. R., Gerecke, D. R., Laskin, D. L., Joseph, L. B., & Laskin, J. D. (2016). Mustard vesicants alter expression of the endocannabinoid system in mouse skin. *Toxicology and Applied Pharmacology*, 303, 30–44. https://doi.org/10.1016/j.taap.2016.04.014
- Won, Y.-S., Kim, J.-H., Lizardo, R. C. M., Min, H.-J., Cho, H.-D., Hong, S.-M., & Seo, K.-I. (2020). The flavonol isoquercitrin promotes mitochondrial-dependent apoptosis in SK-Mel-2 melanoma cell via the PI3K/AKT/mTOR pathway. *Nutrients*, 12(12), 3683. https://doi.org/10.3390/nu12123683

### SUPPORTING INFORMATION

Additional supporting information can be found online in the Supporting Information section at the end of this article.

How to cite this article: Boateng, S. T., Roy, T., Agbo, M. E., Mahmud, M. A., Banang-Mbeumi, S., Chamcheu, R.-C., Yadav, R. K., Bramwell, M., Pham, L. K., Dang, D. D., Jackson, K. E., Nagalo, B. M., Hill, R. A., Efimova, T., Fotie, J., & Chamcheu, J. C. (2023). Multifaceted approach toward mapping out the anticancer properties of small molecules via in vitro evaluation on melanoma and nonmelanoma skin cancer cells, and in silico target fishing. *Chemical Biology & Drug Design*, *00*, e14418. https://doi.org/10.1111/cbdd.14418